Accounting for Confinement Shifts on the Binding Energies of ^{39}K Feshbach Molecules

by

Jared Popowski

B.A., Physics, University of Colorado Boulder

B.A., Mathematics, University of Colorado Boulder

Defense Date: 10/31/2019

Research Advisor: Eric Cornell (Physics)

Honors Council Representative: Jun Ye (Physics)

Committee Member: Kevin Manley (Mathematics)

A thesis submitted to the Faculty of the

University of Colorado in partial fulfillment

of the requirements for the award of

Departmental Honors in the

Department of Physics

2019

This thesis entitled:
Accounting for Confinement Shifts on the Binding Energies of ^{39}K Feshbach Molecules
written by Jared Popowski
has been approved for the Department of Physics

Prof. Eric Cornell

Prof. Jun Ye

Dr. Kevin Manley

Date

The final copy of this thesis has been examined by the signatories, and we find that both the content and the form meet acceptable presentation standards of scholarly work in the above mentioned discipline.

Popowski, Jared (B.A., Physics)

Accounting for Confinement Shifts on the Binding Energies of ^{39}K Feshbach Molecules

Thesis directed by Prof. Eric Cornell

Ultracold ^{39}K gases provide an ideal platform to study quantum few- and many-body systems, due to the high degree of control present in these systems. In particular, Feshbach resonances facilitate a magnetically tunable interaction strength between the atoms in the gas, and allow the formation of two- and three-body bound states, called Feshbach molecules and Efimov trimers respectively. Radio-frequency dissociation spectroscopy of weakly bound Feshbach molecules is one of the most precise ways to characterize the properties of a Feshbach resonance. We apply a numerical method to our Feshbach molecule binding energy data to compute the shift in the molecule's binding energy due to the presence of a confining potential. These simulations are first used to replicate the confinement shift found for ^{6}Li Feshbach molecules by another group, and then to correct our measurement results for the binding energy of ^{39}K Feshbach molecules. The correction of these measurements is necessary for our determination of the Feshbach resonance location with unprecedented accuracy.

Dedication

To my family: LeRoy, Felicia, Zack, Luke, and Levi, for their unconditional love and support.

Acknowledgements

Firstly, I would like to thank my excellent research advisors, Eric Cornell and Jun Ye. I was incredibly lucky to get my position in the Cornell/Ye group during the second semester of my freshman year, and I could not have asked for a better pair of advisors to do physics research under throughout my time as an undergraduate. Eric's fantastic sense of humor always brightens the mood at our lab and group meetings, and his quick wit and ability to explain physics concepts intuitively has made a tremendous impact on the way that I think about physics. Jun's superhuman work ethic and vast knowledge of seemingly every aspect of experimental physics research is hugely inspirational to me, and I hope to emulate the focus and dedication that he shows to his students and his work in my future endeavors.

I would also like to thank the graduate students who served as my mentors in the lab, Roman Chapurin, Xin Xie, and Michael (Vandy) Van de Graaff. Roman's technical knowledge is unmatched, and his clear directions and insight saved me many times from getting stuck on my projects in the lab. Xin's patience and relentless work ethic always encouraged me to push my limits, which I am very thankful for. Vandy is a fantastic teacher who always made himself available to help develop my physics understanding, and his enthusiasm and technical acumen made working alongside him in the lab a true pleasure.

Lastly, and most importantly, I would like to thank my family. I could never thank my parents enough for the sacrifices that they have made to provide for me. Without the support I received over the years from them and my three brothers, I could never have gotten to where I am today.

Contents

Chapter

1 Introduction **1**

2 Two-Particle Scattering and the Theory of Feshbach Resonances **3**

2.1 Two-Particle Scattering Physics 3

2.1.1 Schrödinger Equation for Relative Motion 3

2.1.2 Scattering Potential and Scattering Length for Ultracold Collisions 5

2.2 Basic Physics of Feshbach Resonances and Feshbach Molecules 8

3 Apparatus and Measurement of Feshbach Molecules **12**

3.1 Properties of ^{39}K 12

3.2 Experimental Setup and Preparation of Atoms 14

3.3 Production and Measurement of Feshbach Molecules 16

4 Confinement Shift for Feshbach Molecules in a Trap **22**

4.1 Intuition 22

4.2 Estimating the Confinement Shift 26

4.3 Theory of the Confinement Shift for Two Atoms in a Harmonic Trap 28

5 Testing and Results of My Confinement Shift Program **30**

5.1 Operation of the Program 30

5.2 Testing the Program 32

5.3 Results for the Confinement Shift to our ^{39}K Feshbach Molecules 34

6 Conclusion and Future Directions **46**

Bibliography **47**

Appendix

A Reproducing ^{6}Li Confinement Shift Values **50**

B MATLAB Program for Determining the Confinement Shift **52**

Figures

Figure

2.1 Effective Potential for Two-Particle Scattering 7

2.2 Two-Channel Feshbach Resonance Model 9

2.3 Scattering Length and Dressed State Energy near a Feshbach Resonance 10

3.1 Hyperfine Structure of ^{39}K 13

3.2 Magnetic Moments of ^{39}K $4^2S_{1/2}$ Hyperfine Ground States 14

3.3 Experimental Setup for Generating Ultracold Atoms 15

3.4 CAD Representation of Ultracold Atom Experimental Setup 16

3.5 Magneto-Association of Feshbach Molecules 17

3.6 Initial and Final States for RF Dissociation of Feshbach Molecules 19

3.7 Extracting the Feshbach Resonance Position from RF Dissociation Data 20

4.1 Confinement Shift Conceptual Figure Part a - Free Atom Continuum 23

4.1 Confinement Shift Conceptual Figure Part b - Dissociation of a Feshbach Molecule in Free Space 24

4.1 Confinement Shift Conceptual Figure Part c - Harmonic Confining Potential 25

4.1 Confinement Shift Conceptual Figure Part d - Feshbach Molecule Dissociation in a Harmonic Trap 26

5.1 Original Results for ^{6}Li Confinement Shift [30] 33

5.2 Reproduced ^{6}Li Confinement Shift 34

5.3 Plot of Confinement Shift Results for ^{39}K 35

5.4 Comparing Confinement Shift Plots Between Systems: The ^{6}Li System 37

5.5 Comparing Confinement Shift Plots Between Systems: Our ^{39}K System 38

5.6 Final RF Dissociation Data including the Confinement Shift 40

5.7 Quadratic Fit of Binding Energy Measurements to Extract Approximate Feshbach Resonance Location 42

5.8 Full Fit of our Binding Energy Data, Not Including the Confinement Shift 44

5.8 Full Fit of our Binding Energy Data, Including the Confinement Shift 45

A.1 Original Table of ^{6}Li Confinement Shifts [30] 50

A.2 Reproduced Table of ^{6}Li Confinement Shifts 51

Chapter 1

Introduction

The field of ultracold quantum gases has exploded in recent years, due to the rapid development in laser cooling and trapping technologies that have made production of such gases possible, for which several Nobel prizes have been awarded. The high degree of control and potential for high resolution imaging of atomic systems has firmly established ultracold gases as an ideal platform to study quantum few- and many-body systems. Ongoing research in the field investigates a wealth of exotic quantum many-body phenomena, including high-T_c superconductivity [26], quantum computation [3], and the fractional quantum Hall effect [1, 10]. Many avenues of modern ultracold gas research utilize the systems as quantum simulators of condensed matter systems. For example, ultracold gases placed in optical lattices can serve as a near perfect realization of the Hubbard model, an approximate model used to describe electrons in a solid [18]. In this sense, an ultracold atomic system can serve as an idealized model for the behavior of real solids which is more approachable for theorists to understand and for experimentalists to engineer.

In pursuit of a deeper understanding of light-matter interactions, the invention of laser cooling techniques to reach quantum degeneracy and the development of optical lattices to reach the regime of strongly correlated systems were crucial to establishing the field of ultracold quantum gases [21]. Another revolution in the field was the application of Feshbach resonances, which allow for full tuning of the interparticle interactions via external magnetic fields [8, 21]. Suddenly, it became possible to achieve a clear separation between the relevant length and energy scales in ultracold gases, which opened up the possibility of studying few-body interactions and *universal* physics,

where the macroscopic observables are invariant on the complex microscopic details of the system [6, 12, 30].

In this thesis, we focus on the measurement and correction of the binding energies of Feshbach dimers formed near an intermediate-strength Fano-Feshbach resonance. This research was done as part of a larger effort to study deviations from the concept of universality in few-body physics, where we measured the location of the three-body Efimov ground state and found a significant deviation from the location predicted by van der Waals universality. For more discussion of this work, see [6, 7]. In addition, our Feshbach resonance data is vital information for the JPL/NASA Cold Atom Laboratory (CAL) collaboration, who are interested in performing Efimov studies in microgravity with ultracold ^{39}K gas on the International Space Station (ISS).

In Chapter 2, I begin by describing the relevant two-particle scattering physics before explaining the theory required to describe magnetically tunable Fano-Feshbach resonances and the formation of Feshbach molecules. In Chapter 3, I describe our apparatus used for generating ultracold ^{39}K gas samples, and the specific procedure for producing and measuring Feshbach molecules. In Chapter 4, I present the theory used to describe the confinement shift to interacting atoms in a harmonic trap. In Chapter 5, I describe a MATLAB program that I wrote to calculate the confinement shift, discuss how the program was tested, and present my results for the confinement shift to our molecules. In Chapter 6, I conclude the work presented in this thesis, and give an outlook to future directions for the lab.

Chapter 2

Two-Particle Scattering and the Theory of Feshbach Resonances

I first give a detailed description of two-particle scattering physics, to familiarize us with concepts such as the scattering length that will appear later in this thesis. Then, I present a simplified overview of the physics necessary to describe a Feshbach resonance. For a more comprehensive description of Feshbach resonances, I refer the reader to review papers on the topic [8, 27].

2.1 Two-Particle Scattering Physics

The details of two-particle scattering are covered in many textbooks, including [19] and [22], but some of the basics are presented here in the hope that this thesis can serve as a self-contained introduction to the ultracold atomic physics that we study. The presentation of this section is inspired by Chapter 1 of Benno Rem's 2013 PhD thesis [24], although other references are listed when necessary.

2.1.1 Schrödinger Equation for Relative Motion

We consider two particles of mass m. Their quantum state is described by the Hamiltonian for two particles interacting via a potential $U(|\mathbf{r}_1 - \mathbf{r}_2|)$,

$$H = \frac{\mathbf{p}_1^2}{2m} + \frac{\mathbf{p}_2^2}{2m} + U(|\mathbf{r}_1 - \mathbf{r}_2|). \tag{2.1}$$

For scattering, one aims to solve the time-independent Schrödinger equation (TISE) for this Hamiltonian, and to do so, it proves useful to separate the center of mass motion from the relative motion

by introducing the center of mass (cm) variables

$$\begin{aligned} \mathbf{R}_{cm} &= \frac{\mathbf{r}_1 + \mathbf{r}_2}{2} \\ \mathbf{p}_{cm} &= \mathbf{p}_1 + \mathbf{p}_2 \end{aligned} \tag{2.2}$$

and the relative motion variables

$$\begin{aligned} \mathbf{r} &= \mathbf{r}_1 - \mathbf{r}_2 \\ \frac{\mathbf{p}}{\mu} &= \frac{\mathbf{p}_1}{m} - \frac{\mathbf{p}_2}{m}, \end{aligned} \tag{2.3}$$

where $\mu = m/2$ is the system's reduced mass. Using these coordinates, our system's Hamiltonian can be rewritten as a sum of the center of mass Hamiltonian $\hat{H}_{cm}$ and the relative Hamiltonian $\hat{H}_{rel}$. The solutions of $\hat{H}_{cm}$, which describes the free particle motion of the center of mass of the atoms, are the standard plane waves. We are more interested in the relative motion of the atoms to study scattering, so we focus on that for the rest of this chapter.

The Schrödinger Equation for the relative motion can be written in the form of spherical coordinates,

$$\Big[-\frac{\hbar^2}{2\mu}\Delta_r + U(r) \Big]\psi = E_k \psi, \tag{2.4}$$

where $r = |\vec{r}|$ and $E_k = \hbar^2 k^2/(2\mu)$ is the energy of the relative motion for a scattering state ($E_k > 0$). We can rewrite the Laplacian operator Δ_r in spherical coordinates, which allows us to separate the radial and the angular parts of the wavefunction. The angular part is simply given by the spherical harmonics, and denoting the radial wavefunction by $R_l(r)$, we then introduce $u_{kl}(r) = rR_l(r)$ to simplify the radial part of the Schrödinger Equation. This leaves us with the simplified radial Schrödinger Equation

$$\Big[\frac{d^2}{d^2 r} - \frac{l(l+1)}{r^2} - \frac{2\mu}{\hbar^2}U(r) + k^2 \Big] u_{kl}(r) = 0, \tag{2.5}$$

where l is the orbital angular momentum quantum number. We can interpret this equation to mean that the two particles experience an effective potential given by

$$U_{\text{eff}}(r) = \frac{l(l+1)}{r^2} + \frac{2\mu}{\hbar^2}U(r). \tag{2.6}$$

The significance of l in these formulas can be understood as follows. For a general scattering process in which atoms scatter off of a spherically symmetric potential $U(r)$, we have two components:

(1) An incoming plane wave $\psi^{(0)} = e^{+ikz}$: we use this to represent a free particle instead of the more accurate description of a wave packet, since wave packets are expanded in terms of plane waves.

(2) An outgoing scattered spherical wave $\psi^{sc} = f_k(\theta)e^{ikr}/r$: here $f_k(\theta)$ is the *scattering amplitude*, which depends on the scattering angle θ and the wave number k [30].

Here we made, without loss of generality, the choice of having the wave propagate along the z-axis. In the quantum mechanical description of the process, the incoming plane wave can be decomposed into a superposition of incoming and outgoing spherical waves ("partial waves"), each with a well-defined orbital angular momentum l [19]. We give names to the different partial waves: for $l = 0$ we have s-wave scattering, for $l = 1$ we have p-wave scattering, $l = 2$ is d-wave scattering, and so on.

2.1.2 Scattering Potential and Scattering Length for Ultracold Collisions

All of the previous arguments were made without specifying the particular form of the relative potential $U(r)$. For collisions between two neutral atoms in their ground states, the interatomic potential consists of a short-range potential and a long-range tail provided by the van der Waals interaction [4].

The short-range potential is essentially the electronic Born-Oppenheimer potential, which is the ground-state energy of the electron clouds when the nuclei of the atoms have a fixed separation r [4, 8]. However, the full details of the potential in the short-range region are complicated and unnecessary: the effect of the short-range can be encapsulated by the accumulated phase of the radial wave function at a boundary radius $r = b$ [28]. A simple approximation is to say that the short-range potential is characterized by a hard-core repulsion at $r = b$ (treating the atoms as

completely rigid), so that $U(r) = \infty$ for $r < b$.

For separations much larger than the size of the electron cloud of an individual atom, the interaction energy is dominated by the van der Waals interaction (in the form of induced dipole-dipole interactions) caused by the polarizability of the electron clouds [4, 24]. The van der Waals interaction is described by a $-C_6/r^6$ potential, which has a natural length scale called the *van der Waals length* expressed in terms of the dispersion coefficient C_6: $R_{vdW} = \frac{1}{2}(\frac{2\mu C_6}{\hbar^2})^{1/4}$. For $r \sim R_{vdW}$, the potential energy becomes comparable to the collision energy, so the effect of the potential outside of this region vanishes, and the wavefunction approximates the free space wavefunction.

Altogether, we have that our approximate relation for the relative potential $U(r)$ over all length scales is

$$U(r) = \begin{cases} \infty, & r < b \\ -C_6/r^6, & r > b. \end{cases} \tag{2.7}$$

The effective potential $U_{\text{eff}}(r)$ expressed in equation (2.6) is plotted in Figure 2.1 below for the relative potential (2.7) that we just found and three different scattering channels l: $l = 0, 1$, and 2. The horizontal red line shows the relative motional energy $\hbar^2 k^2/(2\mu)$ of an incoming particle pair in the limit of ultracold collisions ($k \to 0$). In this limit, the waves in the $l > 0$ channels have too little energy to reach the scattering center. Hence, for ultracold collisions, we will only be concerned with s-wave ($l = 0$) scattering, unless otherwise specified.

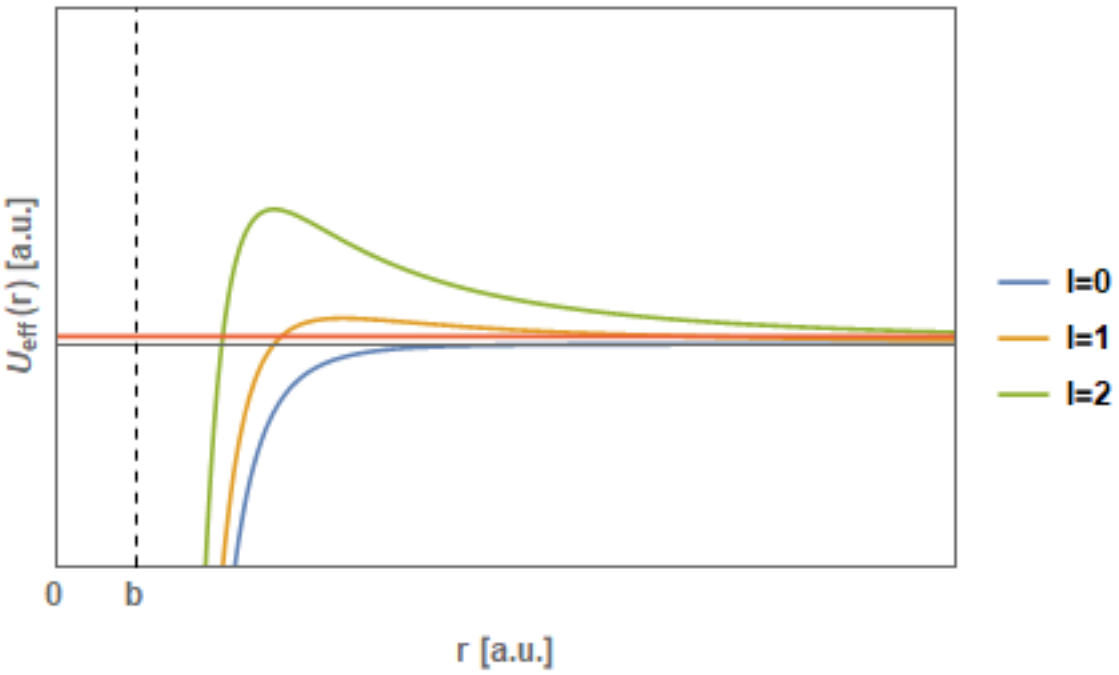

Figure 2.1: The effective potential $U_{\text{eff}}(r)$ for several values of l, where we have taken the relative potential $U(r)$ to be a van der Waals type potential with a hard-core repulsion at $r = b$. Note that the potentials for $l \neq 0$ have a maximum, which creates an effective rotational barrier for particles with a relative energy lower than the maximum. The horizontal red line corresponds to the relative energy of a particle pair in the limit of ultracold collisions $k \to 0$. Therefore, for sufficiently cold gases, only the $l = 0$ (s-wave) scattering contributes to the scattering.

We define the two-body s-wave scattering length a as the negative of the low-energy ($k \to 0$) limit of the scattering amplitude $f_k(\theta)$ that we very briefly mentioned in Section 2.1.1 [24],

$$a \equiv -\lim_{k \to 0} f_k(\theta). \tag{2.8}$$

We will refer to this parameter as the *scattering length* for short. The most important thing about the scattering length for our purposes is not necessarily how it is defined (although that is important): it is the fact that we obtain a useful quantity to describe ultracold collisions when we choose to define a in this way. The scattering length is the most important parameter governing the interactions of low-energy atoms, since it entirely characterizes the asymptotic behavior of the scattering wavefunction in the low energy limit [13]. The absolute value of a is a measure of the

strength of the scattering, and the sign of a tells you whether the scattering wavefunction between the free atoms has a negative derivative ($a > 0$) at the boundary of the potential or a positive derivative ($a < 0$) at the boundary. For a bound state to exist, the wavefunction must have a negative derivative at the potential boundary, so that we can satisfy the boundary condition of an exponentially falling wavefunction outside of the potential that is characteristic of a bound state. Hence real bound states can only form for $a > 0$. Additionally, the effective interactions between atoms are either repulsive ($a > 0$) or attractive ($a < 0$), depending on the sign of the phase shift that the interatomic potential causes to an incoming scattering wavefunction [19, 22].

2.2 Basic Physics of Feshbach Resonances and Feshbach Molecules

Imagine an atom with two molecular potentials, V_{bg} and V_c, which represent two different scattering processes between a pair of the atoms (see Figure 2.2). The molecular potential $V_{bg}(R)$ (where $r = R$ is the radial separation of the atoms) is the potential that two free atoms encounter when coming in from $R \to \infty$, and it is hence the energetically open channel for a collision process having the near-zero energy $E \to 0$. This is why we call V_{bg} the *open channel*, or alternatively the *entrance channel*. The other potential $V_c(R)$ can support a molecular bound state (in Figure 2.2, this bound state has an energy E_c) near the threshold of the open channel. A *Feshbach resonance* occurs when this bound state energetically approaches the asymptotic potential energy $E = 0$ in the open channel, modifying the scattering in the open channel.

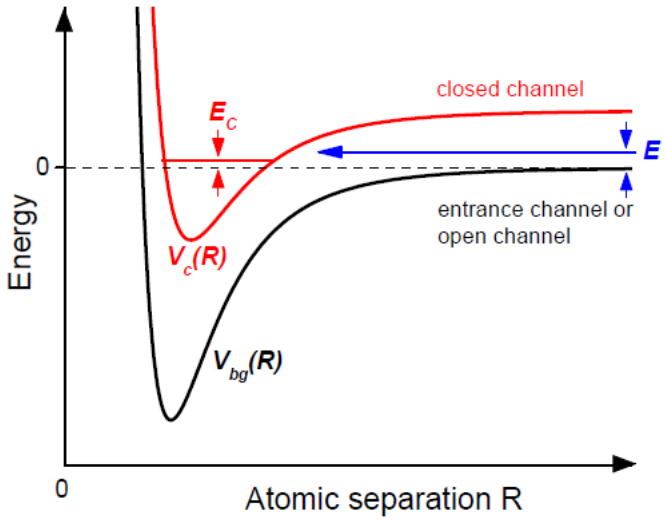

Figure 2.2: A simple two-channel model of a Feshbach resonance. Image obtained from [8].

Hence it is clear that in order to have a Feshbach resonance, we need some way to control the energy difference between the molecular bound state and the collision energy in the open channel. In most cases (including our specific case with ^{39}K), this is obtained by ensuring that the potentials V_{bg} and V_c have different magnetic moments: this allows the energy difference between the two channels to be controlled via a magnetic field. Feshbach resonances in these cases are referred to as *magnetically tuned Feshbach resonances*.

If B is varied so that it passes through a Feshbach resonance, the scattering length a changes dramatically, increasing or decreasing to $\pm\infty$, jumping discontinuously to $\mp\infty$, and then returning to a value close to its original off-resonant value [4]. One can describe a magnetically tuned Feshbach resonance by a simple equation for the s-wave scattering-length a as a function of the applied magnetic field B [20],

$$a(B) = a_{bg}\left(1 - \frac{\Delta}{B - B_0}\right), \tag{2.9}$$

where a_{bg} is the *background scattering length*, B_0 denotes the *resonance position* where the scattering length diverges ($a \to \pm\infty$), and Δ is the *resonance width*, measured in units of the magnetic field. Equation (2.9) is plotted as a function of B in panel (a) of Figure 2.3.

The coupling of the bound state to the open channel threshold creates a coupled state with

energy E. On the $a < 0$ side of the Feshbach resonance, E is positive and the coupled state is "virtual", meaning that it influences the scattering but is not an accessible state. For $a > 0$, the coupled state is a real molecular state, because E is below the continuum. We call such a molecular state a *Feshbach molecule*, or a *Feshbach dimer*. The binding energy of a Feshbach molecule for large positive values of a is approximated by

$$E_b = \frac{\hbar^2}{2\mu a^2} = \frac{\hbar^2}{ma^2}. \tag{2.10}$$

Therefore, in the limit of large positive a, E_b depends quadratically on the detuning $B - B_0$. This results in the bend seen in the inset to panel (b) of Figure 2.3, where we have plotted the dressed state energy E as a function of B near a magnetically tuned Feshbach resonance.

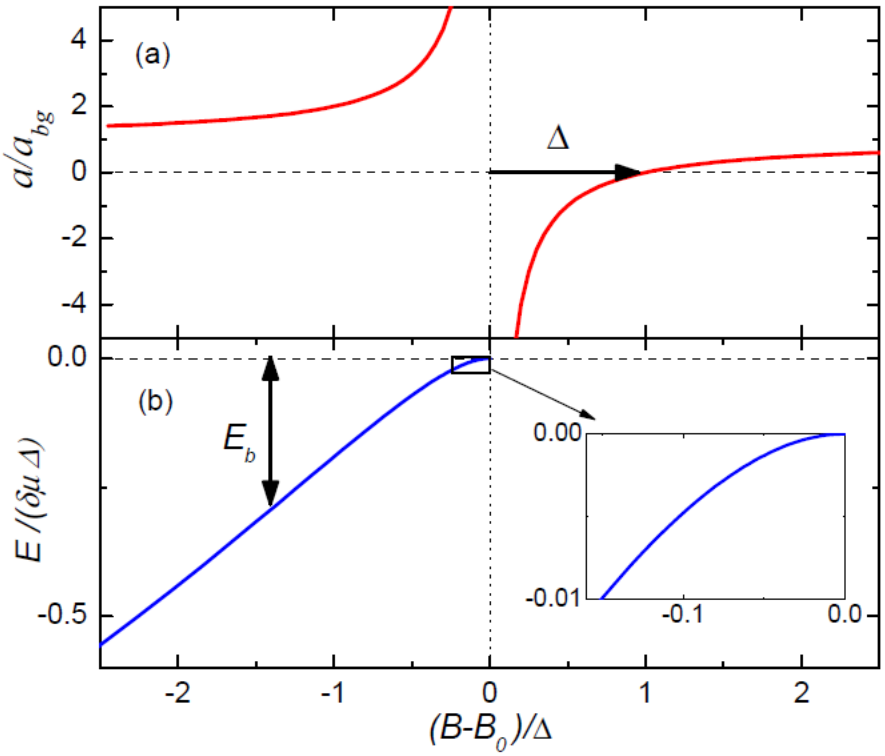

Figure 2.3: A plot (a) of the s-wave scattering length a and (b) of the dressed state energy E near a magnetically tuned Feshbach resonance. The binding energy is defined to be positive, $E_b = -E$. The inset shows the universal regime near the resonance position where a is very large and positive. Image obtained from [8].

The range of B values over which the Equations (2.9) and (2.10) for the scattering length and the dimer binding energy are valid is somewhat complicated, and depends on the specific resonance that one is considering. The scattering length for resonances with large width Δ (conventionally called "broad resonances") typically follows Equation (2.9) over a large fraction of the resonance width. For such resonances the bound state is universal over this large detuning range, and its binding energy is well-described by Equation (2.10). On the other end of the spectrum, resonances with small widths Δ ("narrow resonances") often have smaller ranges of B for which Equations (2.9) and (2.10) are accurate. However, there are exceptions to this general behavior, and a more accurate description of the validity of our expressions for a and E_b requires the introduction of a resonance strength parameter s_{res}. This dimensionless parameter takes into account Δ, a_{bg}, and $d\mu$, the difference in the magnetic moment of the molecule in the closed channel and the free atoms in the open channel [24]. For more information on s_{res}, we refer the reader to [8].

The large a (i.e. $|a| \gg R_{vdW}$) region is of particular interest because of its *universal* properties, in which all physical observables, including all scattering and bound state properties, are determined by the scattering length a. This behavior is deemed universal because it is insensitive to the microscopic details of the problem and the chosen atomic species [7].

A large part of the research that we conducted during my time in the lab was centered on testing the limits to universality in ^{39}K. The discussion in this section has shown that the applied magnetic field provides an experimental fine-tuning parameter that can be used to make $|a|$ arbitrarily large, in particular larger than the natural low-energy length scale R_{vdW} [4]. This shows the extreme usefulness of Feshbach resonances as a means for widely tuning the interaction strength between atoms in an ultracold gas, and in our particular case for testing the limits to universality.

Chapter 3

Apparatus and Measurement of Feshbach Molecules

3.1 Properties of ^{39}K

^{39}K has several properties that make it advantageous for the types of few-body studies that we conduct in the lab. For one, this isotope has very narrow ($\Delta < 0.5$ G) and very broad ($\Delta \sim 50$ G) magnetic Feshbach resonances in several different hyperfine states, which makes feasible the study of resonances that have different properties with the same apparatus [11]. In addition, for certain magnetic field values there exists a particular hyperfine state for which the unitary regime is reached and a different hyperfine state that is noninteracting (i.e. $|a| \to 0a_0$), which allows one to perform radio-frequency (RF) Ramsey spectroscopy between these states to accurately determine two- and three-body interaction parameters within the gas [12].

The hyperfine structure of ^{39}K is shown in Fig. 3.1. Transitions between states can be accomplished with RF radiation (for magnetic dipole transitions) and optical 770 nm (D1) and 767 nm (D2) light. Taking into account the Zeeman splitting of these hyperfine states under an external magnetic field B, we find that RF transition frequencies between $|F, m_F\rangle$ states are $<$ 1GHz for moderate B-fields, which makes our microwave engineering more manageable.

Feshbach resonances occur in the $\left|4^2S_{1/2}, F = 1\right\rangle$ ground states, which are immune from spin-exchange collisions [11]. In particular, we aim to populate our largest and coldest sample of atoms in the $|F = 1, m_F = -1\rangle$ state, which is the only trappable $|F = 1\rangle$ state, since it is the only one with a positive magnetic moment at low B-field values (see Fig. 3.2).

The $|F = 1, m_F = -1\rangle$ state can be magnetically levitated with just a 14 G/cm B-field gradi-

ent near B= 0 G. However, for B-field values B $>$ 82 G, its magnetic moment becomes negative, and the atoms can no longer be trapped (once again, see Fig. 3.2). Therefore, any magnetic trap (in our case, a quadrupole trap, or QT for short) has a finite trap depth $U/k_B = k_B^{-1} \int_{0\text{ G}}^{82\text{ G}} \mu(B) dB = 1.5$ mK for the $|1, -1\rangle$ state. Since this trap is so shallow, we utilize Doppler and sub-Doppler laser cooling techniques to reduce the temperature of our cloud to $\mathcal{O}(10\mu\text{K})$, which sufficiently lowers the evaporation rate ($\sim \exp(-U/k_B T)$) and allows for magnetic trapping [29].

To study quantum few-body physics such as the three-body Efimov effect, we require even lower temperatures $\mathcal{O}(10-100\text{nK})$. To achieve this, we employ an all-optical evaporation technique: evaporation is performed in an optical dipole trap in the presence of an external magnetic field which is tuned near a Feshbach resonance to enhance the elastic collision rate.

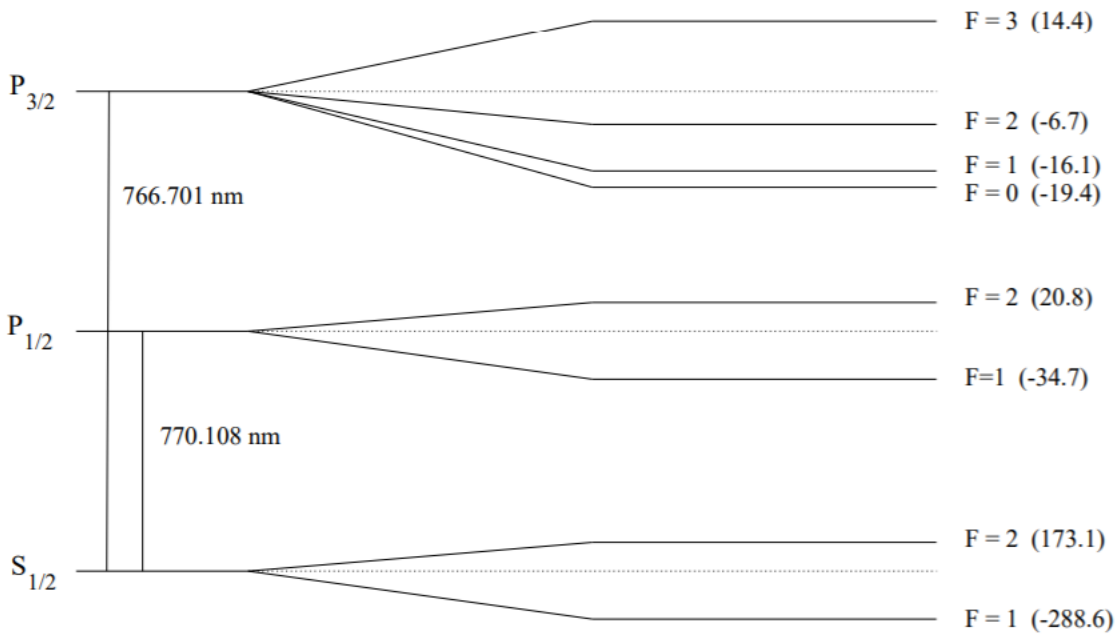

Figure 3.1: The hyperfine structure of ^{39}K at zero magnetic field. Note our condensed notation for the states on the left side: more conventionally, we write the ground state as $4^2S_{1/2}$, and similarly for the other states. Relative splittings (parenthesis) are in MHz. Image obtained from [6].

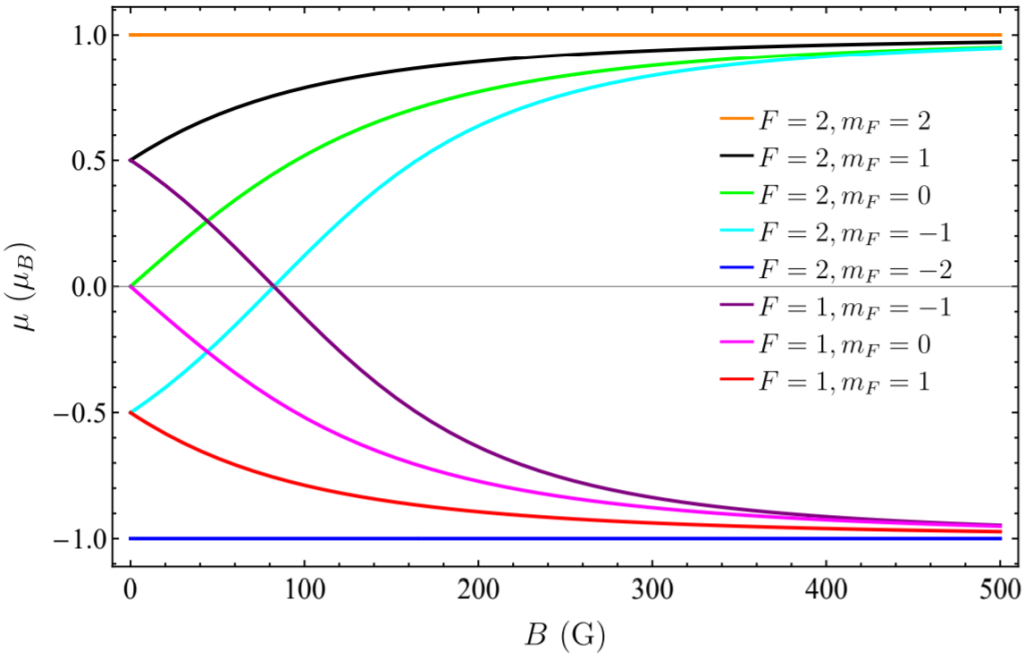

Figure 3.2: The magnetic moment μ of the $4^2S_{1/2}$ hyperfine ground states, where μ is taken as the derivatives of the energies with respect to B (energies are functions of B because of the Zeeman splittings of the hyperfine states) and $\mu_B \approx 1.4$ MHz/G is the Bohr magneton. Image obtained from [6].

3.2 Experimental Setup and Preparation of Atoms

Fig. 3.3 and Fig. 3.4 are images of our experimental cooling setup. Our apparatus consists of a three chamber setup: the first magneto-optical trap MOT1 which contains two "arms" with potassium sources, the MOT2 stainless steel chamber, and a fused silica science cell which has 9 windows.

The procedure for preparing the atoms is fairly straightforward. Potassium vapor from the sources is loaded into MOT1, where it goes through an initial Doppler cooling stage. The atoms are then transferred to the MOT2 chamber via a push beam, which has a linear polarization and whose frequency is red detuned from the D2 transition. Once a sufficient number of atoms is trapped in MOT2, we perform a series of MOT compression and sub-Doppler cooling stages. We then load

the atoms into a quadrupole trap inside an electronically controlled cart, and move the cart over to the science cell. After transferring the atoms from the cart QT to the science QT and returning the cart back to its initial position, we increase the science QT trap confinement and load a fraction of the atoms into an optical dipole trap. Finally, we turn off the QT, turn on a magnetic field bias tuned near a Feshbach resonance to increase elastic collisions, and perform all-optical evaporation, reaching $\mathcal{O}(10 - 100\text{nK})$ final temperatures.

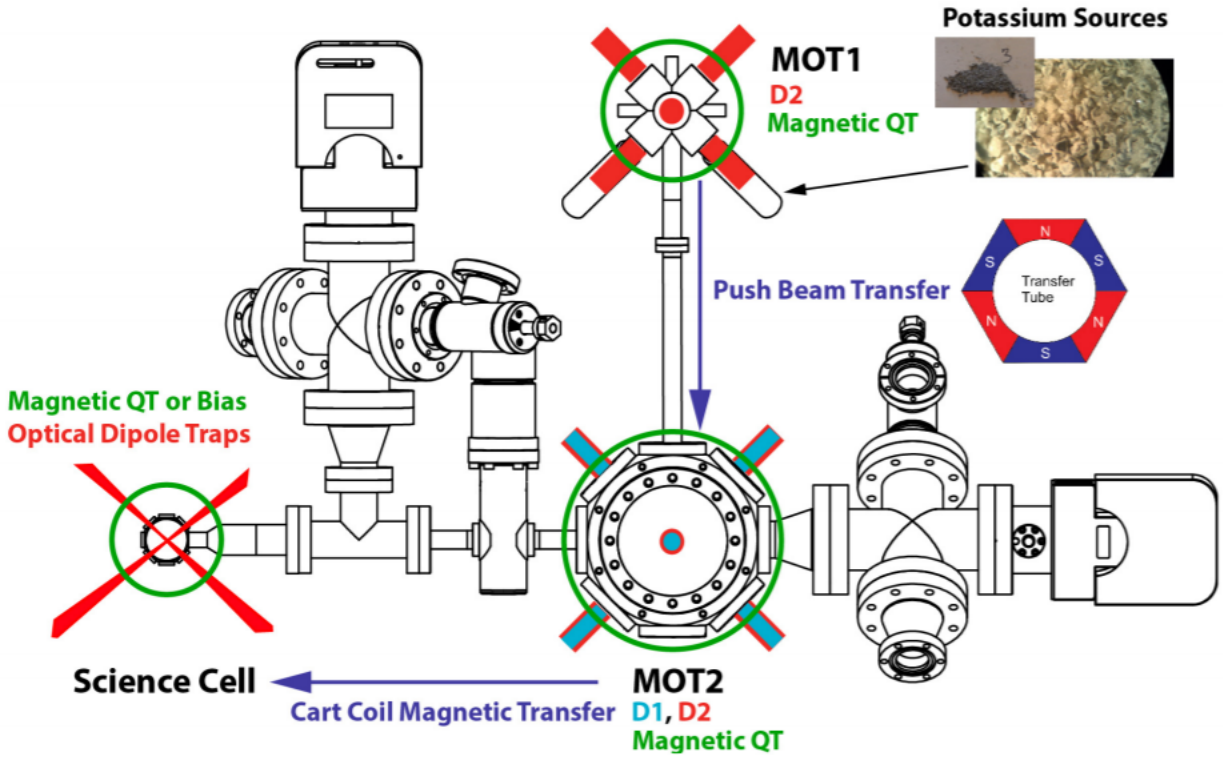

Figure 3.3: A diagram of our experimental cooling procedure. Image obtained from [6].

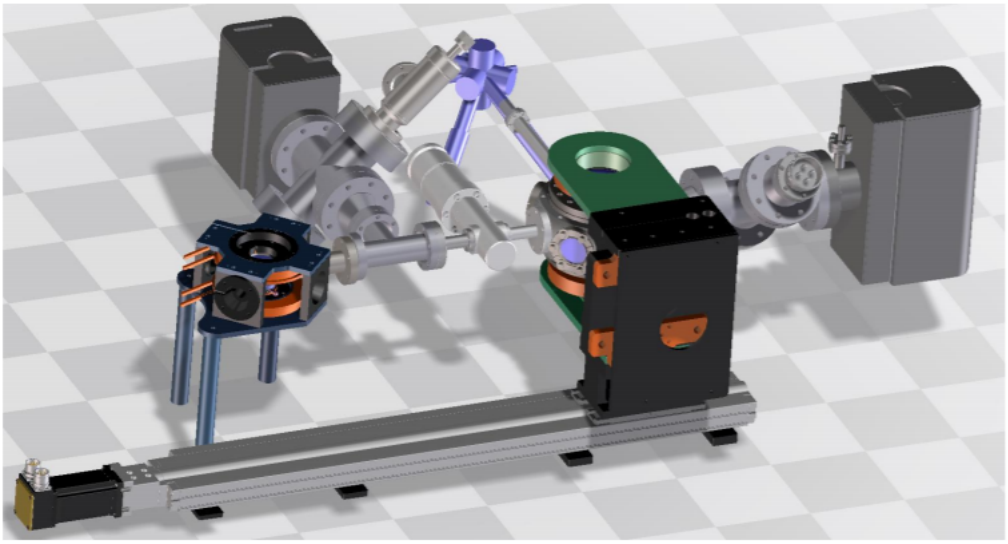

Figure 3.4: A CAD representation of our experimental setup for generating ultracold atoms. Image obtained from [6].

3.3 Production and Measurement of Feshbach Molecules

We use magneto-association [14,23] to create a macroscopic population of Feshbach molecules for our binding energy measurements. This technique has historically resulted in the largest molecular populations; in 2005, a JILA lab measured atom-dimer conversion efficiencies of around 50% for the magneto-association of a ^{85}Rb Bose gas system [15]. However, our current setup is more challenging, and a significant amount of our ^{39}K atoms ($> 80\%$) remain unpaired after the sweep. Since we need $10^3 - 10^4$ Feshbach molecules for an adequate signal for RF spectroscopy, the atomic samples required before the sweep are on the order of $\sim 10^5$ atoms.

Magneto-association is generally accomplished with a time-varying magnetic field near a Feshbach resonance. A slow adiabatic sweep of the magnetic field through the resonance into the region where bound molecules exist causes the association of atoms into very weakly bound Feshbach molecules [14,15]. This makes intuitive sense when we consider that the bound molecular state becomes degenerate with the free atom continuum at the location of the Feshbach resonance. In our experiment, we begin by producing a thermal sample of atoms far from the resonance on

the $a > 0$ side, before rapidly ramping to the $a < 0$ side of the resonance (dashed red arrow on the top in Fig. 3.5). We then form our molecules by slowly sweeping the magnetic field back to the positive side of the resonance, depicted in Fig. 3.5 by the dashed red arrow on the bottom. Finally, we apply a sequence of cleaning pulses to blast away unconverted atoms, leaving behind a pure molecular gas.

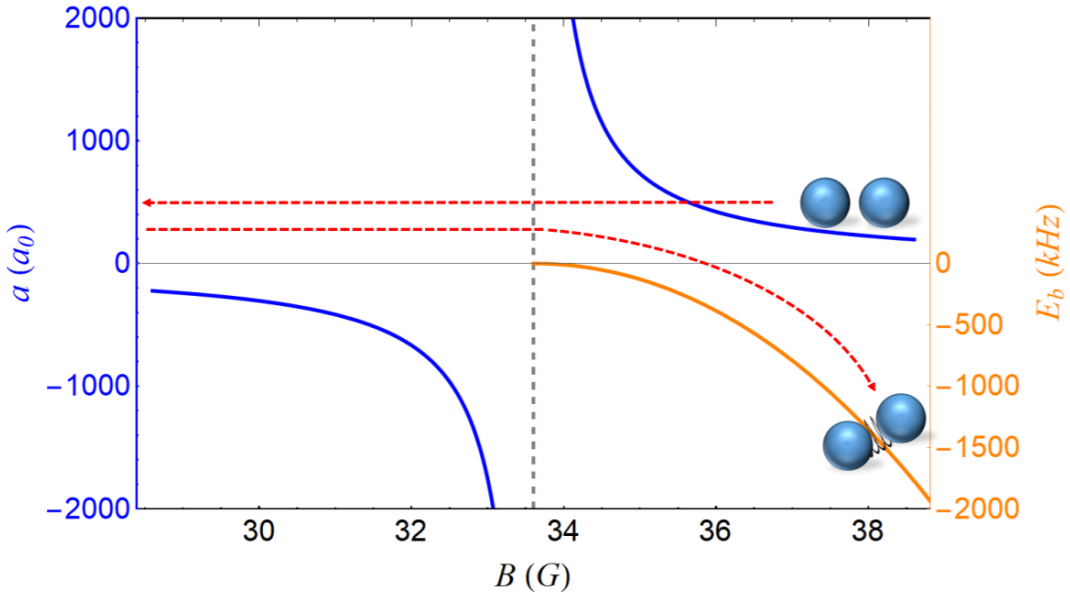

Figure 3.5: A diagram of magneto-association of Feshbach molecules near the $B_0 = 34$ G resonance in the ^{39}K hyperfine state $|F = 1, m_F = -1\rangle$. Two unpaired atoms are adiabatically transferred to the molecular state with magnetic field ramps, which are depicted by the dashed red arrows. Image obtained from [6].

After a pure molecular gas is produced, the magnetic field is ramped to various values, corresponding to different binding energies, where we perform RF dissociation spectroscopy. From these measured binding energies, we can very precisely determine the position and the width of our Feshbach resonance of interest [8]. For sufficiently low molecular densities, the molecular gas can be described as an ensemble of two-atom states, initially in the bound state $|\psi_{mol}\rangle$. The state $|\psi_{mol}\rangle$ has an energy that is E_b less than the energy of two non-interacting atoms in the $|F = 1, m_F = -1\rangle$

hyperfine state, and we use an RF pulse to break the pair by exciting one of its atoms to the $|F = 2, m_F = 0\rangle$ state. This transition is less sensitive to the magnetic field near B values of interest, which allows for long molecular interrogation times and thus high spectral resolution [7]. In addition, the final state $|F = 2, m_F = 0\rangle$ is nearly non-interacting due to its small associated scattering length $a_f = -19a_0 < 0$, where a_0 is the Bohr radius [6]. The measured spectrum is then fit to a functional form given by the Franck-Condon factor, which determines the shape of the dissociation spectra. When these dissociation spectra are paired with B-field measurements obtained by taking atomic lineshapes before and after the dissociation spectroscopy, we can precisely determine the binding energy E_b of our Feshbach molecules along with a corresponding B-field value [6]. The location of the Feshbach resonance is then obtained by plotting the binding energy versus the magnetic field, and extrapolating the resulting functional form of the dependence to $E_b = 0$, where the bound molecular state becomes degenerate with the two free atom continuum (see Figure 3.7). Our measurements are so precise for our intermediate strength Feshbach resonance that they place constraints on the theory used to fit this functional form for the extrapolation.

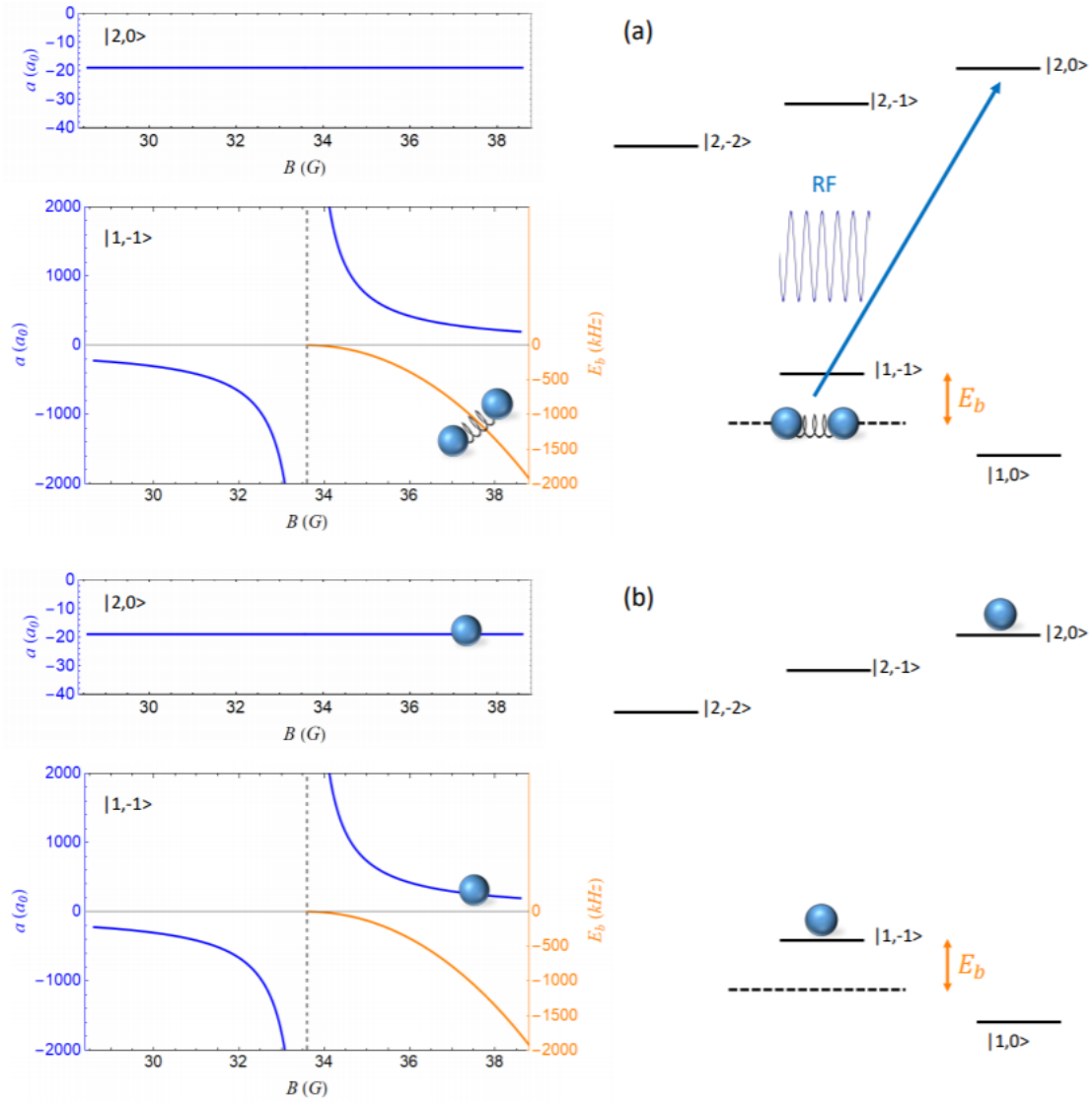

Figure 3.6: A diagram of the initial (a) and final (b) states in our Feshbach molecules RF dissociation procedure. The initial state is a molecular state with binding energy E_b, and the final state has one atom in the $|F = 2, m_F = 0\rangle$ hyperfine state and the other in the state $|F = 1, m_F = -1\rangle$. Image obtained from [6].

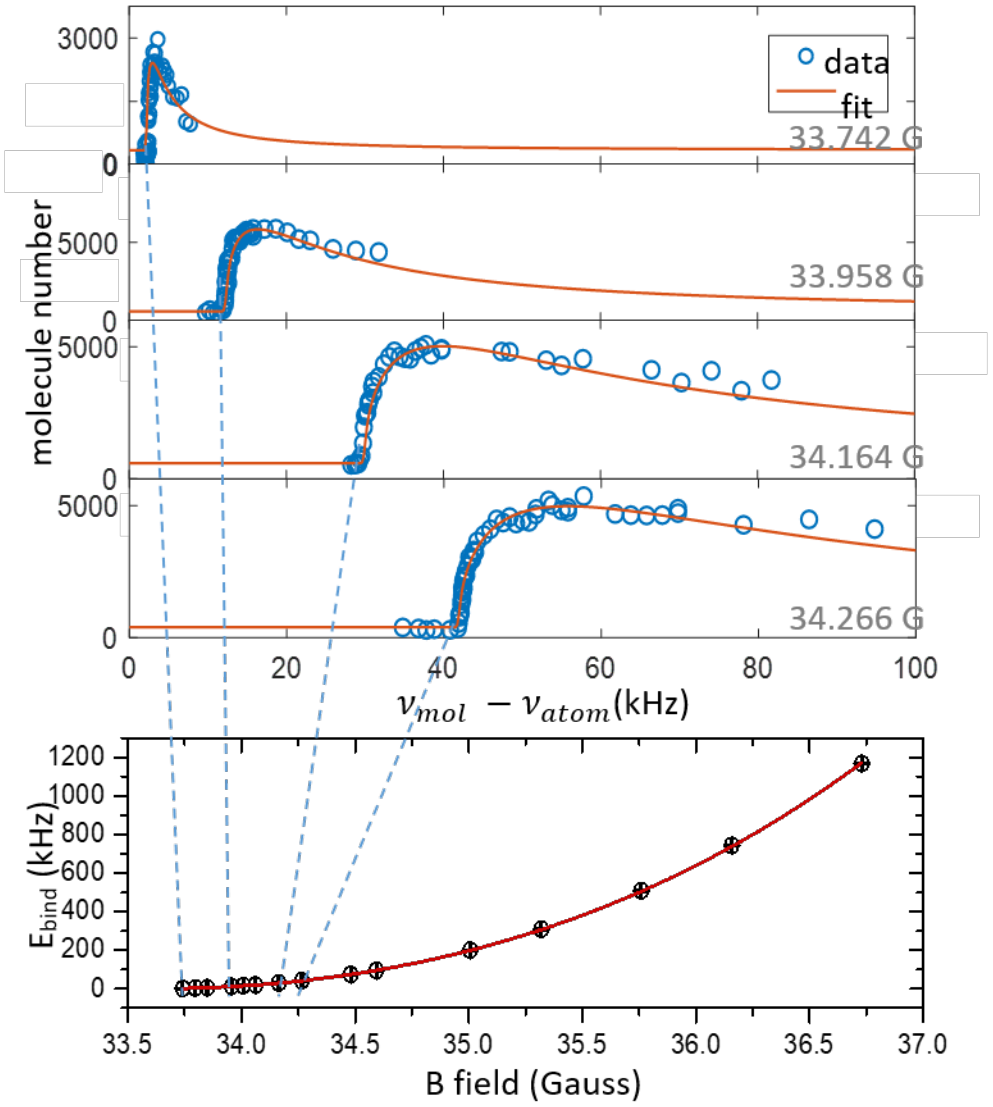

Figure 3.7: A diagram depicting how our Feshbach dimer binding energy data from RF dissociation is used to determine the Feshbach resonance position. A coupled-channel (cc) model is required to fit the data for our intermediate strength resonance (meaning the resonance has an intermediate value of s_{res}, see [8]).

Due to the stability of our magnetic field and high degree of control over other experimental sources of error, our binding energy data has unprecedented precision, and an accurate determination of the Feshbach resonance location requires consideration of additional sources of error. The biggest systematic error affecting our molecular spectra arises from the confining potential, used to

hold the atoms up against gravity. To accurately determine the binding energy of the molecules, we have to subtract the effects of the confining potential from the dissociation frequency $\delta\nu$ [30]. The shift on our measured binding energies due to the confining potential is referred to as the *confinement shift*. Both the initial and final states for the RF dissociation have confinement shifts associated with them, and the total confinement shift is the difference between the final state shift and the initial state shift.

Chapter 4

Confinement Shift for Feshbach Molecules in a Trap

4.1 Intuition

We can understand the confinement shift intuitively by building up a qualitative picture of the effects of confinement on Feshbach molecules. We introduce the relevant physics step-by-step in Figure 4.1.

Part a of the figure depicts the continuum of scattering states available to two free atoms, since they are allowed to have any nonnegative value for the relative motional energy $E = \hbar^2 k^2/(2\mu)$. In free space, where a confining potential is not required to keep the atoms in place, dissociation of a Feshbach molecule with binding energy E_B would involve dissociation into these free atom continuum states. This is represented in part b of Figure 4.1, where we use a van der Waals tail $U(r) = -C_6/r^6$ to represent the molecular potential (ignoring the short-range $1/r^{12}$ repulsive part of the potential for visual simplicity). However, on Earth we need a way to prevent the atoms from falling out of our system under the influence of gravity, and so we introduce a confining potential to hold up the atoms. In part c of Figure 4.1, we show the potential energy and first three energy levels for a harmonic trap $V_t(r) = \frac{1}{2}m\omega^2 r^2$. Once the trap is introduced, the continuum of free atom scattering states that was previously present becomes the discrete energy levels of the trap. However, we note that in practice the experimental resolution may be insufficient to resolve the trap levels, in which cases the final state of dissociation can be well-described by a continuum [30]. Adding together the effects of the molecular potential and the confining potential, we end up with the potential curve depicted in part d of Figure 4.1. In the figure, the dashed navy blue curve gives

the original form of the confining potential, and the dashed light blue curve gives the original form of the molecular potential. The binding energy of a Feshbach molecule with free-space binding energy E_B is perturbed to the new value $E_{B'}$ by the harmonic trap, and similarly the energy levels in the trap that the dissociated atoms occupy are perturbed by the molecular potential.

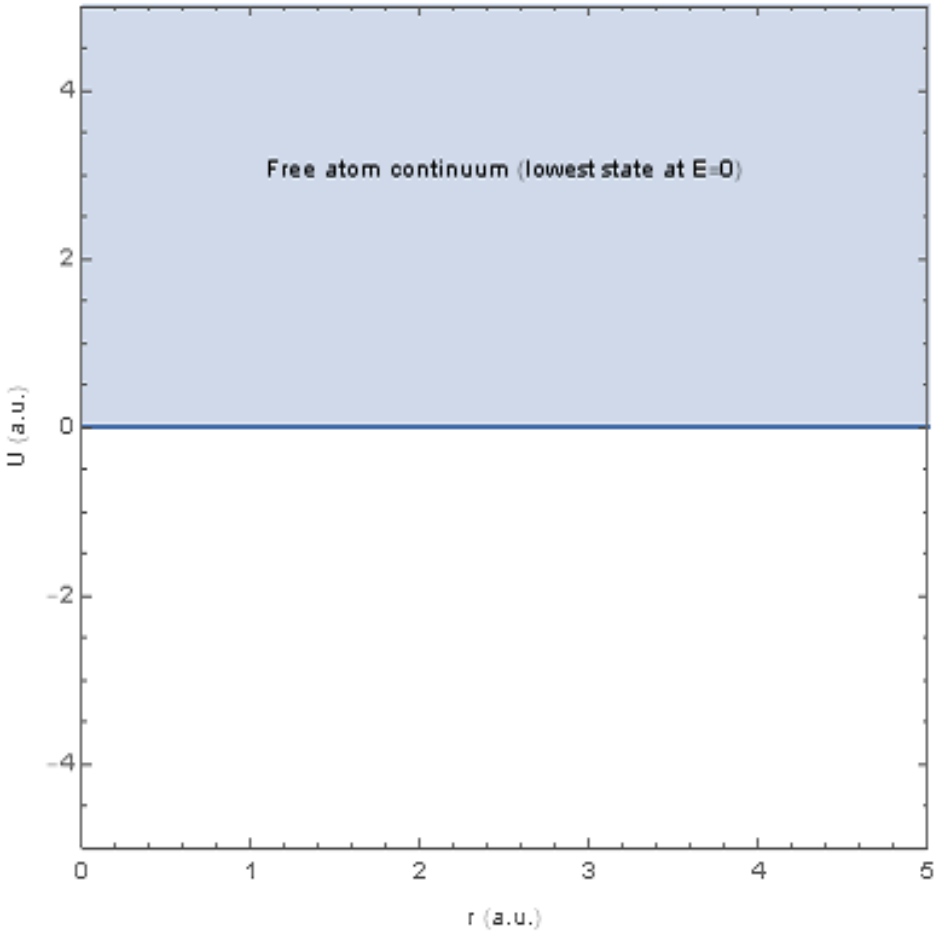

Figure 4.1a: The scattering state for two free atoms can have any nonnegative value for the relative motional energy $E = \hbar^2 k^2/(2\mu)$, with the minimum-energy scattering state occurring for $E = 0$. This means that for two atoms in free space, there is a continuum of scattering states, represented in the plot by a shaded region for $U > 0$. Here r is the interparticle separation.

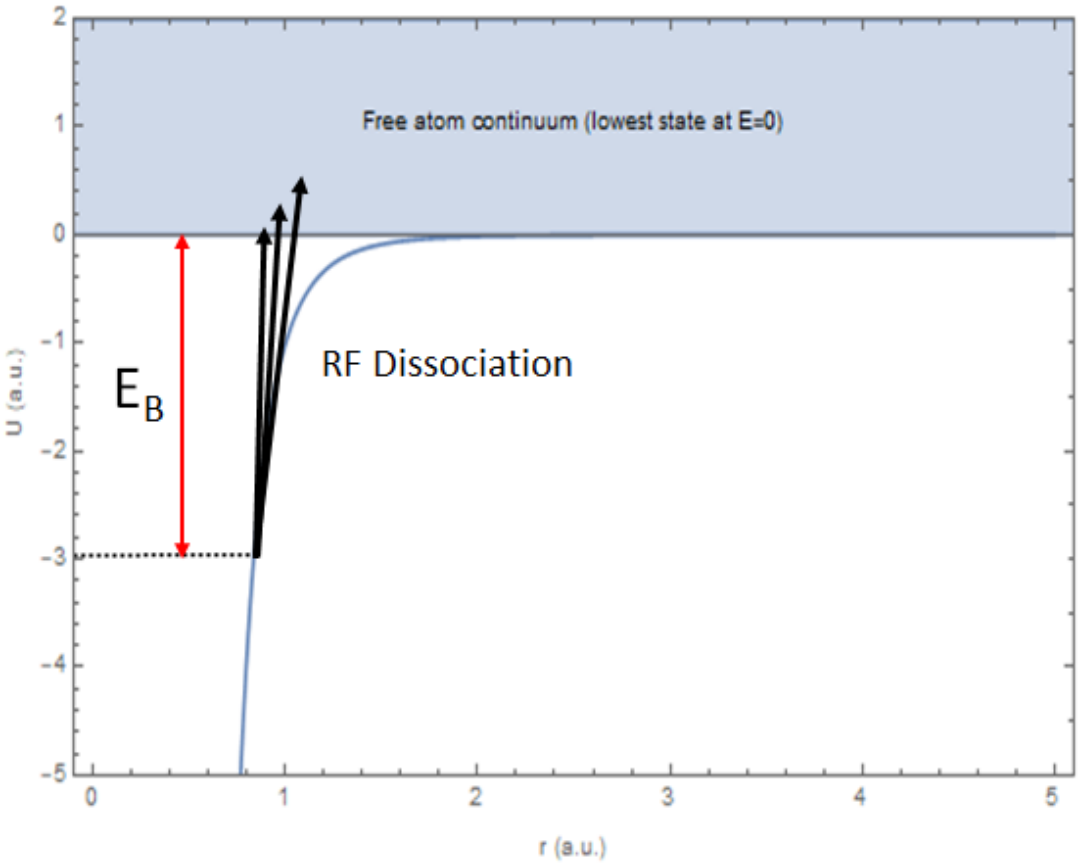

Figure 4.1b: The dissociation of a Feshbach molecule with binding energy E_B in free space, where the blue curve is a van der Waals tail $U(r) = -C_6/r^6$ representing the molecular potential and the final states are the free atom continuum states from the previous part of the figure (r is the interparticle separation). The black arrows illustrate the fact that the molecule does not necessarily have to dissociate into the $E = 0$ state, since there is some probability of dissociating into a higher energy continuum state for a higher frequency RF pulse. This is evidenced by the long tails on our measured dissociation spectra in Figure 3.7.

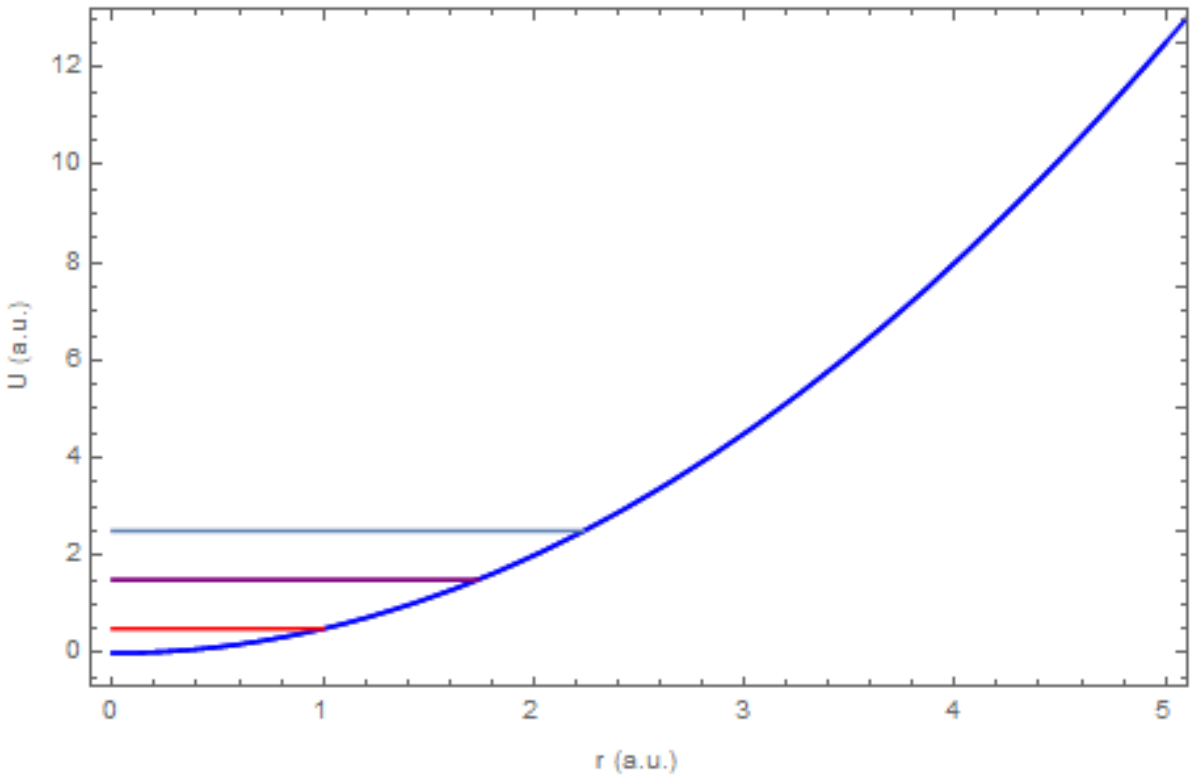

Figure 4.1c: The introduction of a confining potential (here a harmonic potential $V_t(r) = \frac{1}{2}m\omega^2 r^2$) takes the continuous energy spectrum of the scattering states for two free atoms and restricts it to the discrete energy levels of the trap, the first three of which are given in the plot.

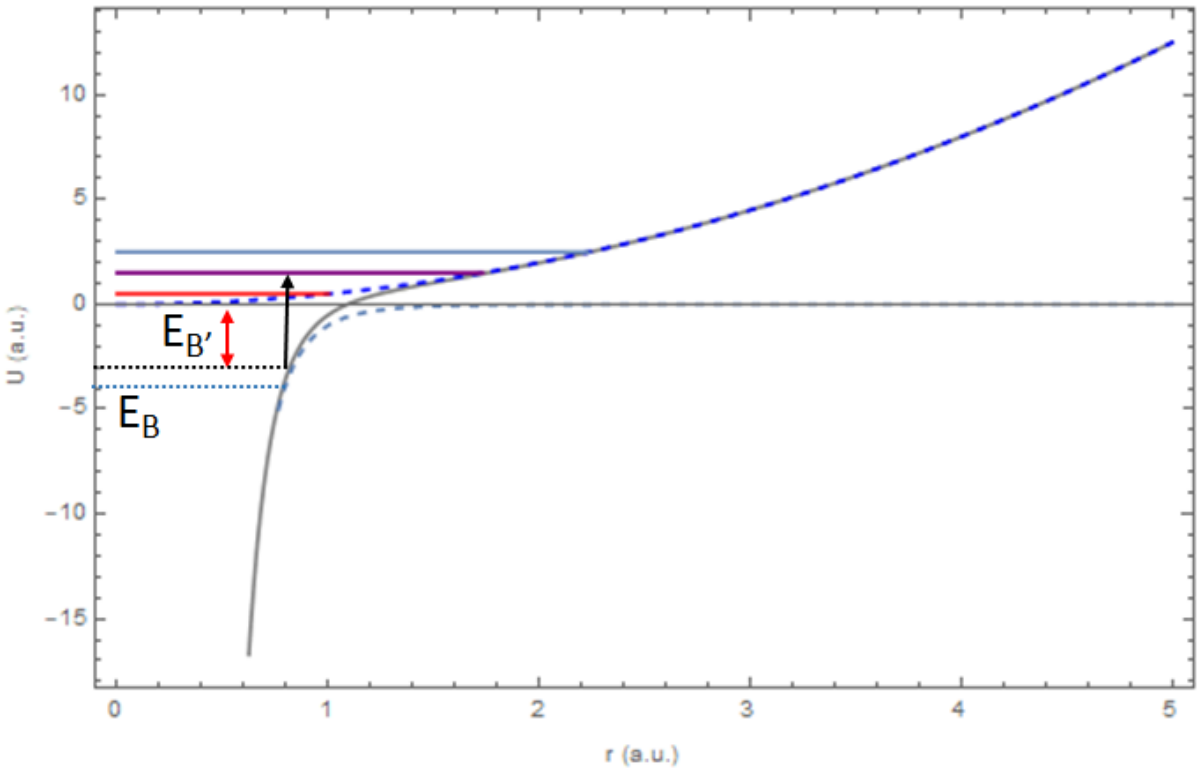

Figure 4.1d: The full story of Feshbach molecule dissociation into a trap, where the molecular potential in part b and the confining potential in part c have been added together. The dashed navy blue curve gives the unperturbed form of the confining potential, and the dashed light blue curve gives the unperturbed form of the molecular potential. The confining potential perturbs the binding energy of a Feshbach molecule from its free space value E_B to the new value $E_{B'}$ (the difference on this plot is exaggerated for clarity), and the molecular potential perturbs the discrete trap states for the final dissociated free atoms.

4.2 Estimating the Confinement Shift

We would like to get an idea of how much the initial and final states are perturbed by. We begin with the final states: dissociation under confinement involves a discrete spectrum of final states with energies approximately given by

$$E_b^{\text{trap}} \approx E_b^{\text{free}} + \hbar(\omega_r + \frac{1}{2}\omega_z) + \hbar(j\omega_r + k\omega_z), \tag{4.1}$$

where $E_b^{\text{free}} = E_b$ is the dimer binding energy measured in free space (whose value we ultimately seek to determine), ω_r and ω_z are the radial and axial trapping frequencies respectively, and j and k are even integers [6]. The first correction term is the zero-point energy E_0 of the trap, which in our case is $E_0/h = 87.3(1.4)$ Hz. This arises because the lowest energy state that we can dissociate to in free space is the state with relative motional energy $E = 0$, but the minimum energy state for dissociation in a trap is the ground state of the trap, with energy given by the zero-point energy. The second correction term describes the excited harmonic states, which must be symmetric (i.e. j and k must be even) due to the symmetry of the initial molecular state, but generally these excited states are not resolved by us [6]. Hence, we approximate the confinement shift to our final free atom state by the zero-point energy $E_0/h = 87.3(1.4)$ Hz of our trap.

Since the confining potential is very weak over the range of the Feshbach molecule, we can obtain a rough estimate for the initial confinement shift by applying first-order perturbation theory to our system. In general, the first-order energy correction is given by the matrix element

$$E_n^{(1)} = \left\langle \psi_i^{(0)} \right| H' \left| \psi_i^{(0)} \right\rangle, \tag{4.2}$$

where $\left|\psi_i^{(0)}\right\rangle$ is the unperturbed initial state and H' is the weak perturbation Hamiltonian. The bound initial state of our system has a spatial extent of order $\mathcal{O}(a)$ and is well-described by the universal wavefunction for a weakly-bound Feshbach molecule [9]

$$|\psi_i(a, r)\rangle = \sqrt{\frac{2}{a}} e^{-r/a}, \tag{4.3}$$

where r is the relative distance between the atoms. We then treat the perturbation Hamiltonian H' as the trap potential $V_t(r)$. To the lowest order our trap is quite harmonic, so we make the approximation $V_t(r) = \frac{1}{2} m \overline{\omega}^2 r^2$, where $\overline{\omega} = 2\pi(117.3 + 28.64 + 28.64)/3\ s^{-1} = 365.6\ s^{-1}$ is the average angular trapping frequency of our trap. The first-order energy correction to the bound state at a positive scattering length a is then

$$E_n^{(1)} = \int_0^\infty \frac{2}{a} e^{-2r/a} \frac{1}{2} m \overline{\omega}^2 r^2 dr. \tag{4.4}$$

Plugging in the mass of ^{39}K, our trap's value for $\overline{\omega}$ from above, and a typical scattering length for our experiment of $1000a_0$ (a_0 is the Bohr radius), then dividing the result by Planck's constant h, we find that our estimate for the confinement shift to our initial state is about .009 Hz. Admittedly, we have made several approximations to obtain this answer, but the actual value that we have obtained is not really the important part: we note simply that our estimate for the total confinement shift, obtained by taking the difference between our estimates of the final state shift and the initial state shift, is entirely dominated by the final shift consisting of the zero-point energy of the trap, 87.3 Hz. We will see this same behavior when we compute the actual confinement shifts for ^{39}K in the next chapter.

4.3 Theory of the Confinement Shift for Two Atoms in a Harmonic Trap

While Equation (4.1) for the final state shift and our perturbation theory approach for the initial state shift provide good intuition for the confinement shift, they are only approximations, and do not describe the true energy spectrum of an interacting two-body quantum system in a trap. To obtain the accurate confinement shift on our measurements of ^{39}K Feshbach molecules, we require some more theory.

We consider two interacting atoms of mass m confined in an axially symmetric harmonic trap with axial frequency ω_z and transverse frequency $\omega_\perp$. Just as we did in the beginning of Chapter 2, we introduce the relative and center of mass variables $\vec{r} = \vec{r}_1 - \vec{r}_2$ and $\vec{R}_{cm} = (\vec{r_1} + \vec{r_2})/2$ respectively, and separate the total Hamiltonian into a sum of the center-of-mass part $\hat{H}_{cm}$ and relative part $\hat{H}_{rel}$. We only need to consider the relative motion, since the solutions of the center of mass part (which describe the motion of the center of mass of the atoms in the harmonic trap) are the usual harmonic-oscillator wave functions. The Hamiltonian of the relative motion is

$$\hat{H}_{rel} = -\frac{\hbar^2}{2\mu}\nabla_r^2 + \frac{\mu}{m}V_{trap}(\vec{r}) + V_{int}(\vec{r}), \tag{4.5}$$

where $\mu = m/2$ is the reduced mass, $V_{trap}(\vec{r})$ is the trapping potential

$$V_{trap}(\vec{r}) = \frac{m}{2}(\omega_\perp \rho^2 + \omega_z z^2) \tag{4.6}$$

where $\rho^2 = x^2 + y^2$ is the axial distance in cylindrical coordinates, and $V_{int}(\vec{r})$ is the interaction potential between the atoms. Assuming s-wave scattering, we can model the interaction potential by the Fermi psuedopotential [16]:

$$V_{int}(\vec{r}) = \frac{4\pi\hbar^2 a}{m}\delta(\vec{r})\frac{\partial}{\partial r}r, \tag{4.7}$$

with a denoting the s-wave scattering length.

One can then nondimensionalize the Hamiltonian by expressing all lengths in units of $d = \sqrt{\hbar/(\mu\omega_z)}$ and all energies in units of $\hbar\omega_z$. The eigenfunctions $\Psi(\vec{r})$ and eigenenergies E for the relative motion are then found from the Schrödinger equation, by decomposing $\Psi(\vec{r})$ into the complete set of the harmonic oscillator wave functions. Following this procedure, a 2006 PRA paper by Zbigniew Idziaszek and Tommaso Calarco [17] found the following expression determining the energy levels for $m = 0$,

$$-\frac{\sqrt{\pi}}{a} = \mathcal{F}(-\mathcal{E}/2), \tag{4.8}$$

where

$$\mathcal{F}(x) = \int_0^\infty dt\left(\frac{\eta e^{-xt}}{\sqrt{1-e^{-t}}(1-e^{-\eta t})} - \frac{1}{t^{3/2}}\right) \text{ for } x > 0. \tag{4.9}$$

Here $\eta = \omega_\perp/\omega_z$ is the aspect ratio of the system and $\mathcal{E} = E - E_0$ denotes the energy shifted by the zero-point oscillation energy $E_0 = 1/2+\eta$. This is the main result that we were interested in, as this gives us the shifted energy levels due to confinement in an axially symmetric harmonic trap. The validity of the integral representation (4.9) is limited to $\mathcal{E} < 0$, which is sufficient for our purposes, but this result can be extended to energies $E > E_0$ through analytic continuation [17].

Chapter 5

Testing and Results of My Confinement Shift Program

To calculate the confinement shift to the measured binding energies of our Feshbach molecules, I wrote a MATLAB program that numerically solves Equations (4.8) and (4.9). In the following sections, I describe how the program works, what I did to test the program, and the final results for the confinement shifts to our measured ^{39}K binding energies. I have included the full program in Appendix B for reference.

5.1 Operation of the Program

It is most straightforward to solve Equation (4.9) for a particular value of the confined molecular binding energy E, by plugging into the equation the corresponding value of $x = -\mathcal{E}/2 = -(E - E_0)/2$ and numerically integrating. The corresponding scattering length a is then easily found by using Equation (4.8). In other words, given E, it is relatively simple to find the scattering length a. However, our experimental data necessitates the opposite direction: we have binding energy data for particular values of the scattering length a, and we want to extract the confinement shift to the binding energies $E - E_b$ at these particular a values (here E_b is the universal bound state energy in free space, Equation (2.10)).

To solve this problem, the program has the following basic procedure: we input the particular scattering length a for which we want the confinement shift and an array of energies (the number of points, starting point, and ending point for this array are all controllable parameters). The program finds the scattering length corresponding to each value in the energy array according to

Equations (4.8) and (4.9), and prints out an error message if the scattering length of interest is not close enough to any of the computed scattering lengths, indicating that some parameter defining the energy array must be changed in order to find the correct confinement shift. Otherwise, the program outputs the confinement shift in kHz that must be subtracted from the measured RF dissociation frequency at the scattering length of interest.

To go into more detail, the inputs to the MATLAB program are as follows:

(1) The scattering length a at which the Feshbach molecule RF dissociation measurement was made, stored in the variable testscatter.

(2) The starting point of the energy range over which we want to compute the confined molecular binding energy curve, expressed in units of $\hbar\omega_z$ and stored in the variable Estart.

(3) The ending point of the energy range over which we want to compute the confined molecular binding energy curve, expressed in units of $\hbar\omega_z$ and stored in the variable Eend. Note that since the integral (4.9) is only valid for $\mathcal{E} = E - E_0 < 0$, Eend cannot exceed the zero-point energy of the trap E_0.

(4) The number of energy points between Estart and Eend in the energy range for which we want to find the confined molecular binding energy curve, stored in the variable numEpoints.

The program then numerically solves the integral (4.9) for each energy value from Estart to Eend, for a total of numEpoints values for $\mathcal{F}(-\mathcal{E}/2)$, and the corresponding scattering lengths a are calculated with Equation (4.8). Afterwards, the resulting confined binding energy curve (in units of $\hbar\omega_z$) versus -1/a is plotted, where a is the scattering length measured in units of the oscillator length $1/\sqrt{\hbar/(\mu\omega_z)}$. The universal Feshbach dimer binding energy expression given by Equation (2.10) is also plotted for the same scattering length values on the same plot.

If the experimental a value for which we want to compute the confinement shift does not fall within 0.1 of any of the computed scattering lengths after this process, which could occur either

because the energy range given to the program was too narrow or because the energy grid was too coarse, the program displays the error message "ERROR: Chosen scattering length outside of given energy bounds. Increase the energy bounds in the program (Estart,Eend, and/or numEpoints) to include the scattering length." Otherwise, the program linearly interpolates between the confined and universal energies corresponding to the computed scattering lengths which are nearest to the a value of interest. This gives us the confined and free space binding energies at the desired a value. The difference between these interpolated energies (divided by Planck's constant) is the confinement shift in kHz that we are interested in, which the program prints out.

5.2 Testing the Program

We are not the first experiment to reach the level of precision where the effect of the confinement shift must be accounted for: a 2013 work detailed in reference [30] used the method of RF dissociation to measure a Feshbach resonance location in ^{6}Li with unprecedented precision, and included the effects of the confining potential by solving Equations (4.8) and (4.9) for their system, just as we aim to do. Hence a good test for my MATLAB program is whether it reproduces the results that the authors of reference [30] obtained for the confinement shift, when I give the program all of the necessary trap parameters ($\eta = 10$) and constants for ^{6}Li.

The full tables of the numerical confinement shift results from reference [30] and from my own program are given in Appendix A. In short, my program successfully reproduced the confinement shifts found in [30] for all values of the measured binding energies, with discrepancies much smaller than the experimental errors on the measurements. A plot of the confined vs universal free space binding energies from reference [30] and the corresponding plot from my own program are depicted in Figures 5.1 and 5.2, respectively.

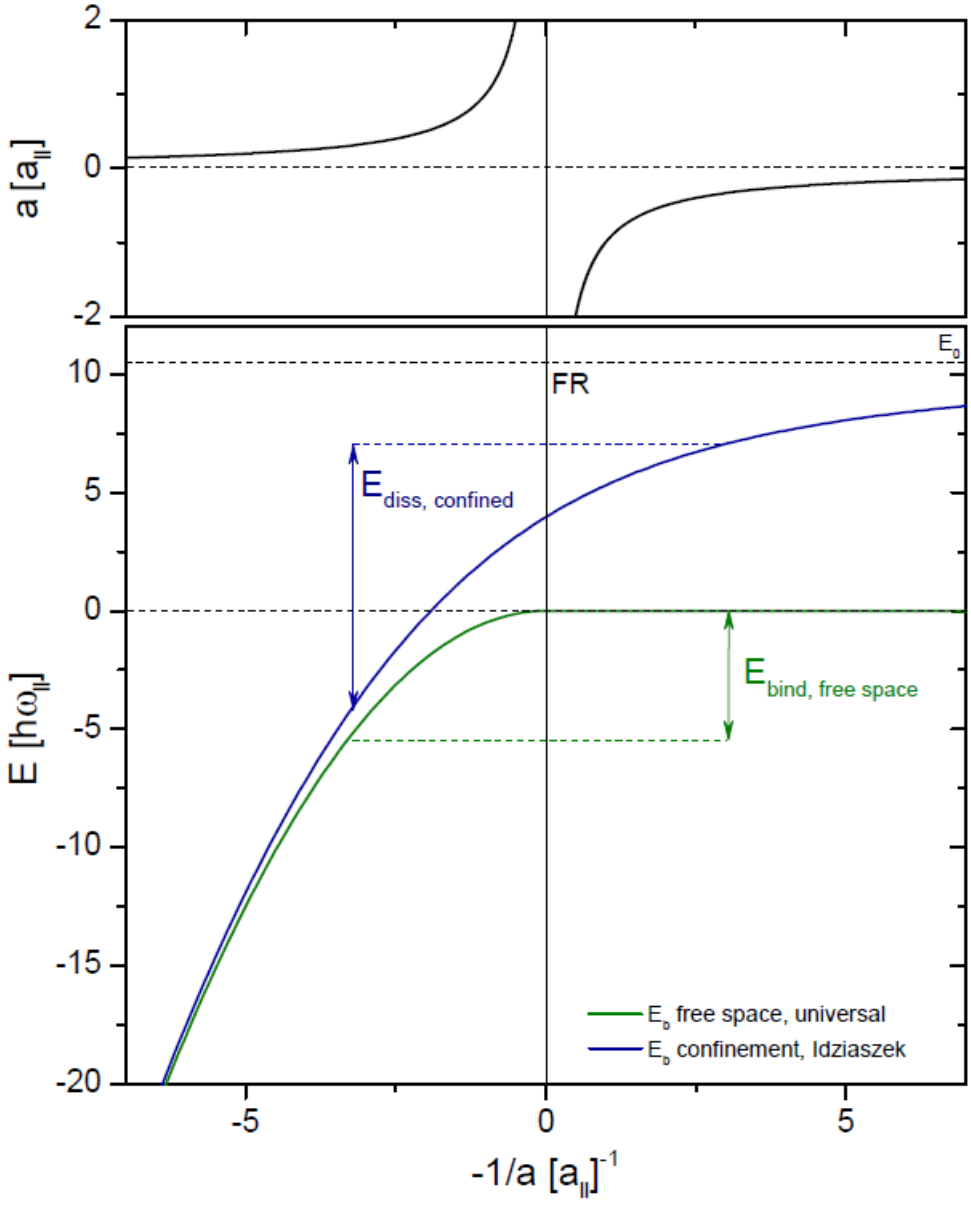

Figure 5.1: The original results for the free space (green) and confinement (blue) ^{6}Li Feshbach molecule binding energy curves. At the point where the scattering length diverges at the Feshbach resonance (FR, upper panel) the universal bound state reaches the continuum. The blue curve shows the universal bound state in the presence of confinement, computed according to [17] with an aspect ratio of $\eta = 10$. The blue arrow represents an RF transition from a molecule at $a > 0$ to two atoms with $a < 0$, where the final state is below the zero-point energy E_0 for large a due to strong interactions between the atoms in this region. The energy units are $\hbar\omega_{||} = 2\pi\hbar\nu_{||}$ and the length units are the oscillator length $a_{||} = \sqrt{\frac{\hbar}{\mu\omega_{||}}}$. Aside from the slightly larger range for Figure 5.2, the axes for this plot and Figure 5.2 are exactly the same (i.e. the units are the same, $\omega_z = \omega_{||}$). Figure reproduced from the Supplemental Materials of [30].

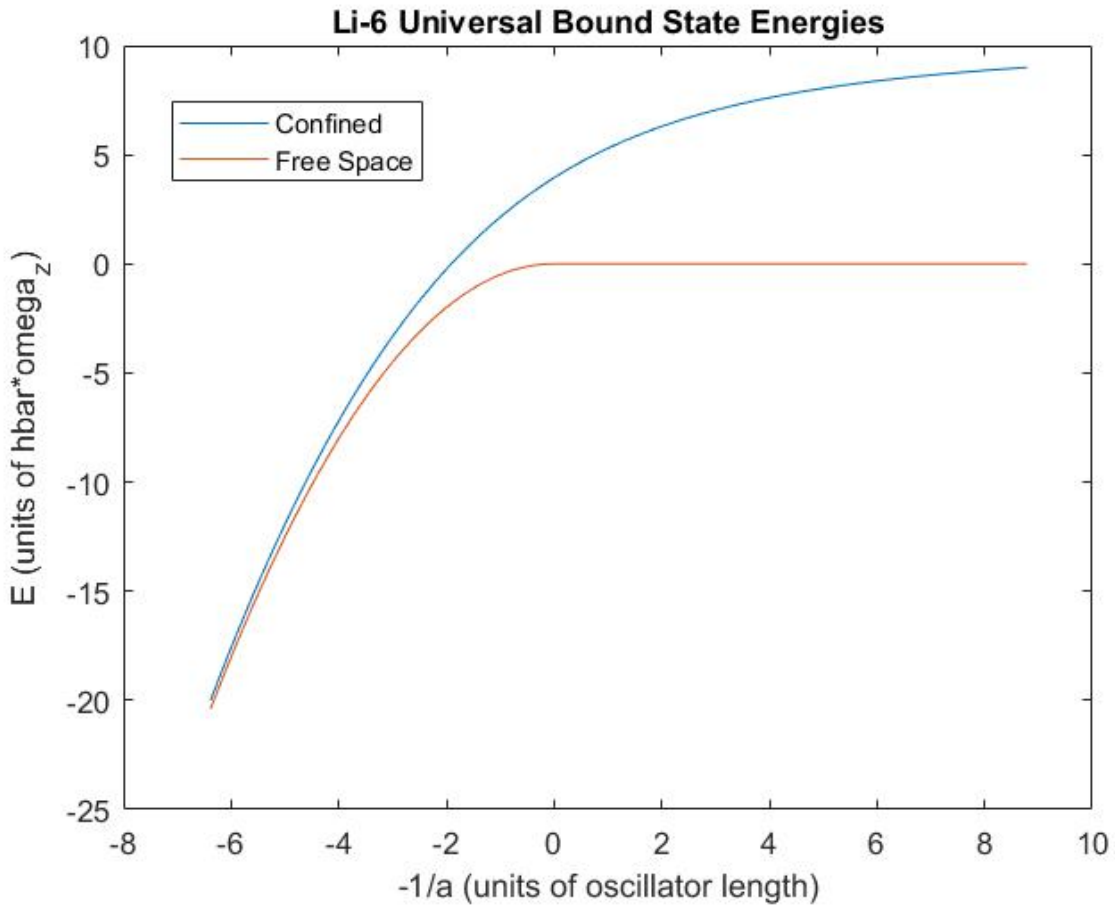

Figure 5.2: The output of my program for the comparison between the free space and confinement ^{6}Li Feshbach molecule binding energies. The energy units are $\hbar\omega_z = 2\pi\hbar\nu_z$ and the length units are the oscillator length $a_z = \sqrt{\frac{\hbar}{\mu\omega_z}}$. Aside from the slightly larger range for my plot, the axes for both Figure 5.1 and this plot are exactly the same (i.e. the units are the same, $\omega_z = \omega_{||}$).

5.3 Results for the Confinement Shift to our ^{39}K Feshbach Molecules

After verifying that my program was able to reproduce the confinement shifts found for the ^{6}Li binding energy data, we needed to do the same procedure to find the confinement shifts for our own ^{39}K binding energy data. Our trap is axially symmetric with a radial trap frequency $\omega_r/2\pi = 28.64(66)$ Hz in the (x, y)-plane and an axial trap frequency of $\omega_z/2\pi = 117.3(1.0)$ Hz, so the trap aspect ratio is $\eta = \omega_r/\omega_z \approx 0.244$. Using this value and the relevant constants for ^{39}K, we

obtained the free space and confined binding energy curves displayed in Figure 5.3.

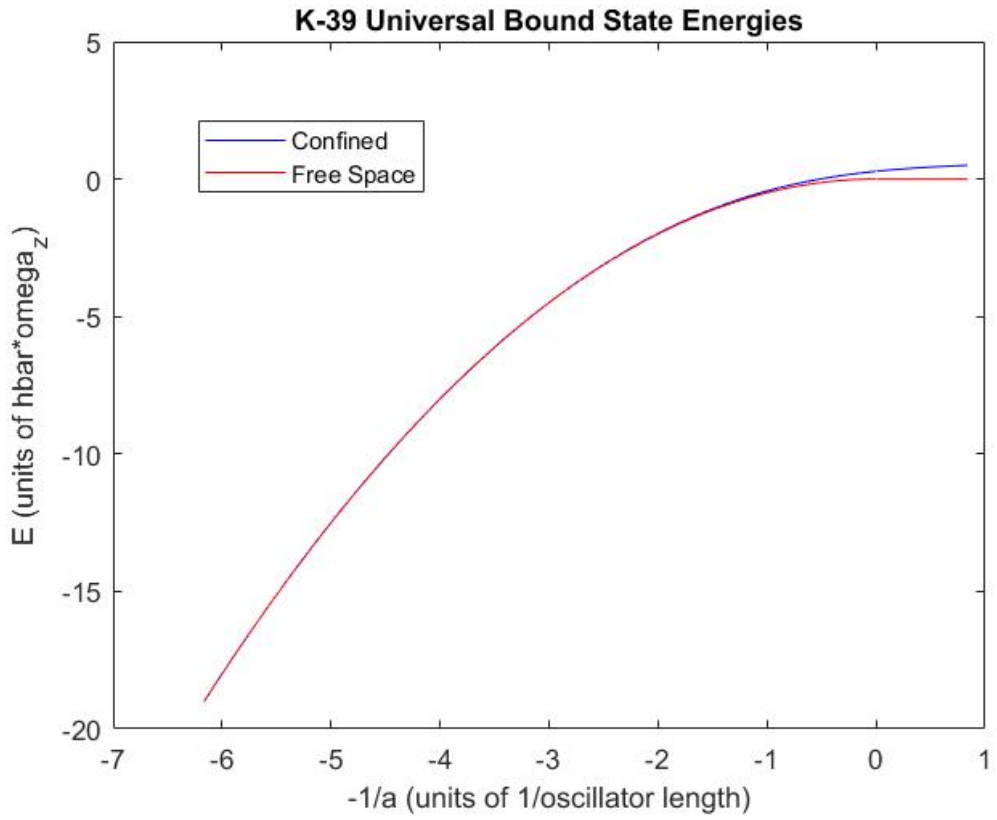

Figure 5.3: The computed free space and confined ^{39}K Feshbach molecule binding energies. The energy units are $\hbar\omega_z = 2\pi\hbar\nu_z$ and the length units are the oscillator length $a_z = \sqrt{\frac{\hbar}{\mu\omega_z}}$.

The clearest difference between Figures 5.2 and 5.3 is that the confined and free space curves in Figure 5.3 coincide for a much longer range of scattering length values than the corresponding ^{6}Li curves in Figure 5.2. It is tempting to attribute this difference to the difference in atomic species, since the mass of ^{39}K atoms is relatively large when compared with ^{6}Li. However, we must be careful about the units of the axes for these plots, since both the x- and y-axes are expressed in dimensionless units which depend on the configuration of the trap, in particular the axial frequency ω_z. Our trap is quite different from the trap used by the group that studied ^{6}Li: our aspect ratio of $\eta \approx 0.244$ means that our trap is "hockey puck" shaped, whereas the group that studied ^{6}Li had a "pencil-shaped" trap with their aspect ratio of $\eta = 10$. To better understand the difference

between Figures 5.2 and 5.3, we must produce equivalent plots that are expressed in units which are less dependent on the trap aspect ratio. One way to accomplish this is to make the dimensionless units for the axes depend on the average trap frequency $\omega_{\text{avg}} = (\omega_x\omega_y\omega_z)^{1/3}$ rather than the trap frequency ω_z for a single axis.[1] This is done in Figures 5.4 and 5.5, respectively, where the energy is now expressed in units of $\hbar\omega_{\text{avg}}$ and the $-1/a$ axis is expressed in units of one over the harmonic oscillator length $a_{\text{h,avg}} = \sqrt{\hbar/(\mu\omega_{\text{avg}})}$, calculated with ω_{avg} instead of ω_z.

We find that the ^{6}Li and ^{39}K plots now look nearly identical, with only slightly different dimensionless zero-point energies (represented by horizontal dashed magenta lines in the figures). This is in spite of the fact that the aspect ratios of the two systems are very different, the typical zero point energy of our trap is about 4.2 times smaller than that of the ^{6}Li group's trap, and the masses of the two atomic species differ by a factor of about 6. To interpret this result, we note that the zero-point energy is approximately proportional to ω_{avg},

$$E_0 = \frac{\hbar}{2}(\omega_x + \omega_y + \omega_z) \approx \frac{3\hbar}{2}\omega_{\text{avg}}. \tag{5.1}$$

Hence, when the energy and length units of our plot are expressed in terms of ω_{avg}, we are essentially normalizing the plots by the zero-point energy. The difference in aspect ratios between the two traps caused the difference between Figures 5.2 and 5.3 because we were normalizing everything with the frequency ω_z, which is much less than the more relevant frequency ω_{avg} in the case of the ^{6}Li pencil shaped trap, and is much greater than ω_{avg} in the case of our ^{39}K hockey puck shaped trap. The fact that Figures 5.4 and 5.5 look virtually the same for the units involving ω_{avg} means that the zero-point energy is the primary quantity that matters when trying to understand how confinement affects the binding energies.

[1] Whether we choose the arithmetic mean or the geometric mean of the trap frequencies for ω_{avg} does not substantially change the final plots or the conclusions that we draw from them.

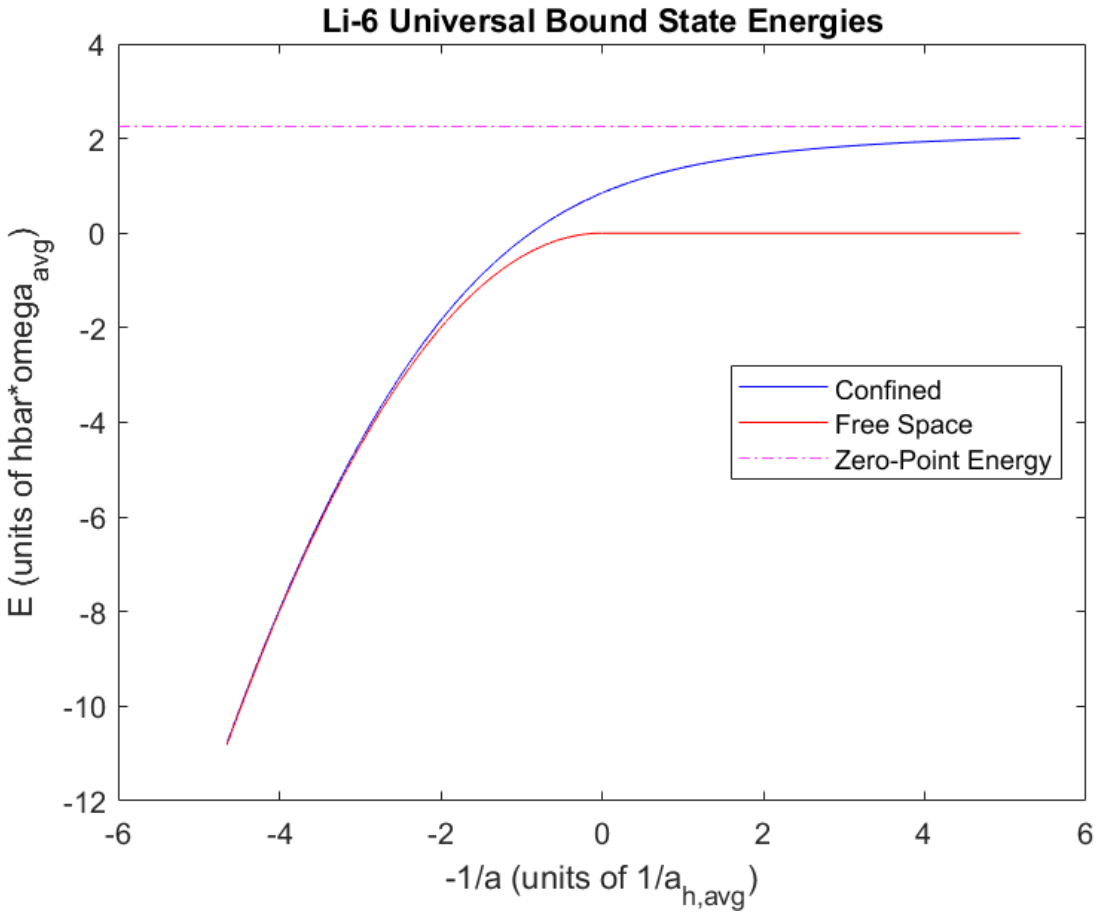

Figure 5.4: The computed free space and confined ^{6}Li Feshbach molecule binding energies, where the units of both axes depend on the the geometric mean trap frequency ω_{avg}: the energy units are $\hbar\omega_{\text{avg}}$ and the length units are the harmonic oscillator length $a_{\text{h,avg}} = \sqrt{\hbar/(\mu\omega_{\text{avg}})}$ calculated with ω_{avg}. Notice how choosing to plot with these units makes these binding energy curves look virtually the same as Figure 5.5, the corresponding plot for our ^{39}K system. For this system, $\omega_{\text{avg}} = 162.1$ s^{-1}, and the dimensionless zero point energy is $E_0 = 2.26$.

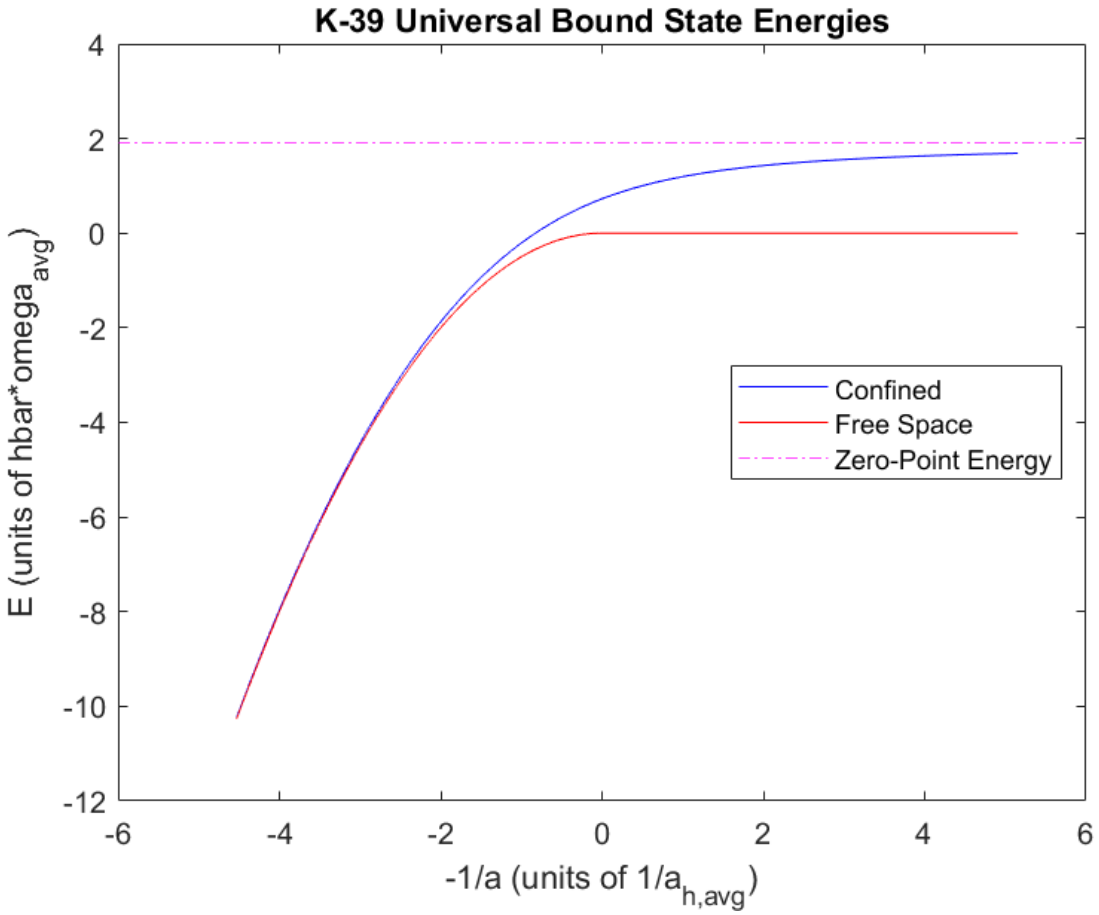

Figure 5.5: The computed free space and confined ^{39}K Feshbach molecule binding energies, where the units of both axes depend on the the geometric mean trap frequency ω_{avg}: the energy units are $\hbar\omega_{\text{avg}}$ and the length units are the harmonic oscillator length $a_{\text{h,avg}} = \sqrt{\hbar/(\mu\omega_{\text{avg}})}$ calculated with ω_{avg}. Notice how choosing to plot with these units makes these binding energy curves look virtually the same as Figure 5.4, the corresponding plot for the ^{6}Li system. For this system, $\omega_{\text{avg}} = 45.82$ s^{-1}, and the dimensionless zero point energy is $E_0 = 1.90$.

We reiterate that both the initial and final states of the RF dissociation have confinement shifts associated with them, and that the total confinement shift is the difference between the final state shift and the initial state shift. With my program, we determined that the confinement-related energy shift of the initial dimer binding energy (with respect to the universal free space relation in Equation (2.10)) is relatively small: 0.7 Hz for $a = 10^4 a_0$ ($E_b \sim 0.9$ kHz), and even smaller for

decreasing values of a (increasing values of E_b). We note in particular that for $a = 1043a_0$, we found a confinement shift of .0457 Hz, which agrees within an order of magnitude with our rough first-order perturbation theory estimation of the confinement shift from the last chapter of .009 Hz at $1000a_0$. Such a small shift of the molecular state energy is primarily because our confining trap is very weak over the scale of the molecules in the center of the trap.

For the final state $|F = 2, m_F = 0\rangle$ after dimer dissociation, the associated scattering length $a \approx a_{bg} = -19a_0$ is very small compared to the harmonic oscillator length (corresponding to very far out to the right in Figure 5.3), so the confinement-related energy shift of our final state is essentially equal to the zero-point energy of our trap, $E_0/h = 87.3$ Hz.

Therefore, the total confinement-related shift is similar for all of our measurements and is approximately equal to the zero-point energy $E_0/h = 87.3$ Hz, to within 1.4 Hz uncertainty on our trapping frequencies. We subtract the total confinement shift from the measured dissociation threshold frequency to extract the dimer binding energy E_b/h in free space; see Figure 5.6 for our final binding energy results.

corresponding B–field (G)	mol. threshold $f_{\mathrm{D}} - \bar{f}_A$ (kHz)	free-space E_b/h (kHz)
33.7420(3)	2.190(56)	2.103(56)
33.7978(4)	3.989(78)	3.901(78)
33.8494(5)	6.095(85)	6.008(85)
33.9575(3)	12.274(57)	12.187(57)
34.0078(4)	15.708(67)	15.621(67)
34.0622(7)	20.139(122)	20.052(122)
34.1644(4)	29.919(83)	29.832(83)
34.2663(6)	41.847(103)	41.760(103)
34.4812(4)	74.382(93)	74.295(93)
34.5940(4)	95.395(137)	95.307(137)
35.0060(5)	200.293(406)	200.205(406)
35.3198(5)	308.716(436)	308.628(436)
35.7593(6)	508.003(582)	507.916(582)
36.1582(7)	742.262(1071)	742.175(1071)
36.7303(5)	1167.324(1031)	1167.237(1031)

Figure 5.6: The final results for the measured molecular dissociation threshold frequency $f_D - \bar{f}_A$, which corresponds to the dimer binding energy in a trap, and the free-space dimer binding energy E_b/h, where we have subtracted the total confinement shift computed with my program from the dissociation threshold frequency. These frequencies were obtained at particular values of the B-field, determined by averaging measured atomic lineshape centers before and after the molecular dissociation measurements. Image obtained from [6].

One would be justified in questioning whether a shift of $\sim$ 87 Hz is really important for measured binding energies on the scale of $1 - 1000$ kHz. In fact, this does turn out to be a meaningful shift to our data. To demonstrate the importance of accounting for the confining potential, we now investigate how the Feshbach resonance location one extracts from a fit of the data depends on whether or not the confinement shift has been subtracted from the data.

Recall from Chapter 2 that E_b for Feshbach molecules depends quadratically on the detuning $B-B_0$ in the limit of large positive a. Large positive a corresponds to very weakly bound molecules, so we can fit our weakest binding energy data from Figure 5.6 to the functional form

$$E_b = C(B - B_0)^2 \tag{5.2}$$

to extract the approximate Feshbach resonance position B_0. In this case, B_0 and the constant of proportionality C are the two fit parameters. We perform this fit for both the measured molecular dissociation threshold frequencies $f_D - \bar{f_A}$ (the data before subtracting out the confinement shift) and the free-space dimer binding energy values E_b/h (the data after subtracting out the confinement shift), to obtain the difference between the extracted resonance positions. Visually, the fit looks identical in both cases, since the confinement shift is so small; we therefore only include a plot of the fit for the data before subtracting out the confinement shift ($f_D - \bar{f_A}$) in Figure 5.7 below. The exact difference between the resonance positions for the two fits depended slightly on the number of points included in the fit; for 4 points the confinement shift increased the resonance location by 3.9 mG (from 33.5865 G without the confinement shift to 33.5904 G with the confinement shift), and for 6 points the confinement shift increased the resonance location by 3.4 mG (33.5862 G without the confinement shift, 33.5896 G with the confinement shift). These differences are greater than our experimental resolution of 1.4 mG, so although this was an approximate method for determining the resonance location, it is clear that accounting for the confining potential gives us a noticeable shift.

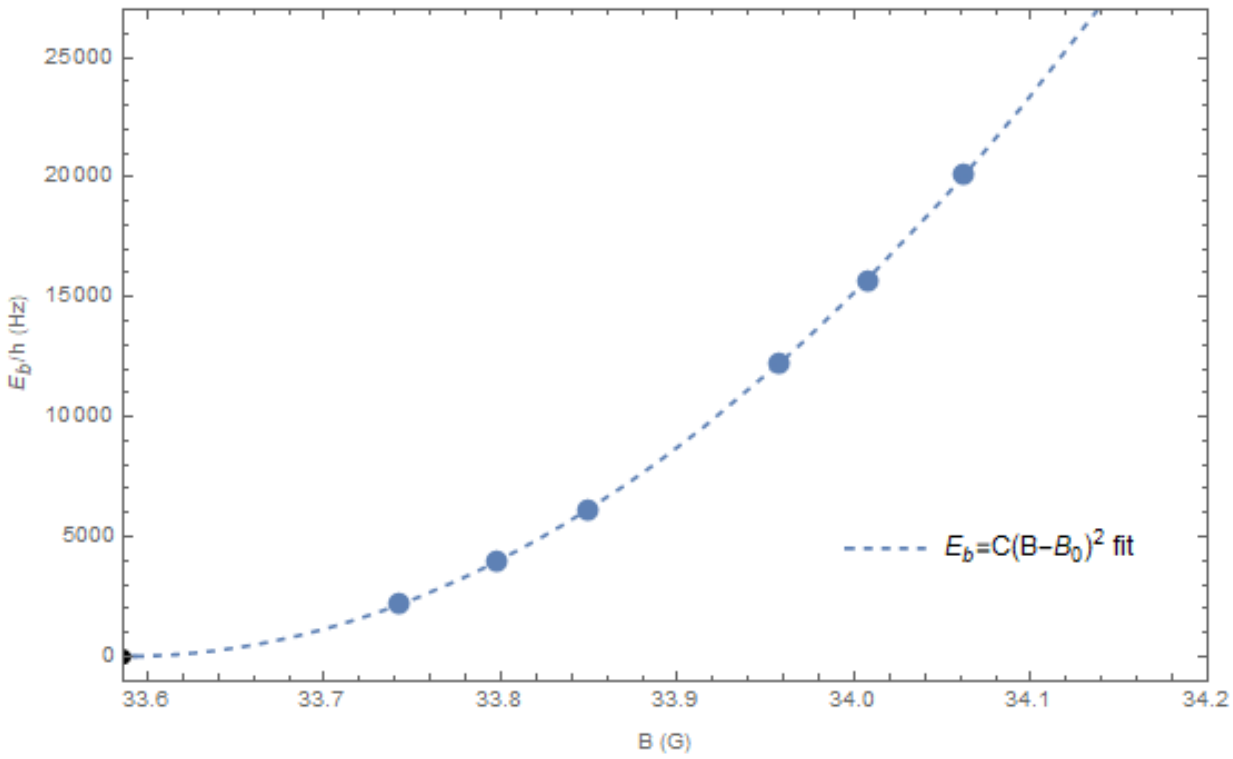

Figure 5.7: A fit of our six weakest binding energy measurements $f_D - \bar{f_A}$ (blue points) to the universal functional form $E_b = C(B - B_0)^2$ (dashed line), where C is the constant of proportionality and B_0 is the Feshbach resonance position in G. The value of $B_0 = 33.5862$ G extracted from the fitted location where $E_b = 0$ is marked as a black point.

We now turn to the full fit of our precision Feshbach dimer binding energy data to a coupled-channel model, to see how accounting for the confining potential affects the fit of our entire data. The fit is given in Figure 5.8, where Figure 5.8a ignores the effects of the confinement shift and Figure 5.8b accounts for the confinement shift to our data. The inset for both of the plots shows our remarkably small fractional residuals, which express the difference between our experimental points and the fitting curve. We plot the fractional residuals because our binding energy data has a large dynamic range. The smaller the fitting residual is (i.e. the closer to zero it is), the better quality the fitting has, and the more certain we can be about our determination of the Feshbach resonance location from the extrapolation of this fit.

We notice systematically negative fit residuals for our smallest E_b data in Figure 5.8a, which is due to the confinement shift in the binding energy of the molecules. Accounting for the confinement shift corrects these systematic shifts in our residuals, aligning nearly every point within the error bars of zero fractional residual, as depicted in Figure 5.8b. This builds confidence in the resonance location extracted from our precision binding energy data. From the fit in Figure 5.8b, we determined the location of our Feshbach resonance to be $B_0 = 33.5820(14)$ G, an improvement of two orders of magnitude over the previous measurement of this resonance, $B_0 = 33.64(15)$ G [25]. In addition, considering that our 1.4mG uncertainty in the resonance location is so much less than the 54.772 G width of our resonance, our scattering length values have unprecedented accuracy relative to previous measurements in many atomic species [30].

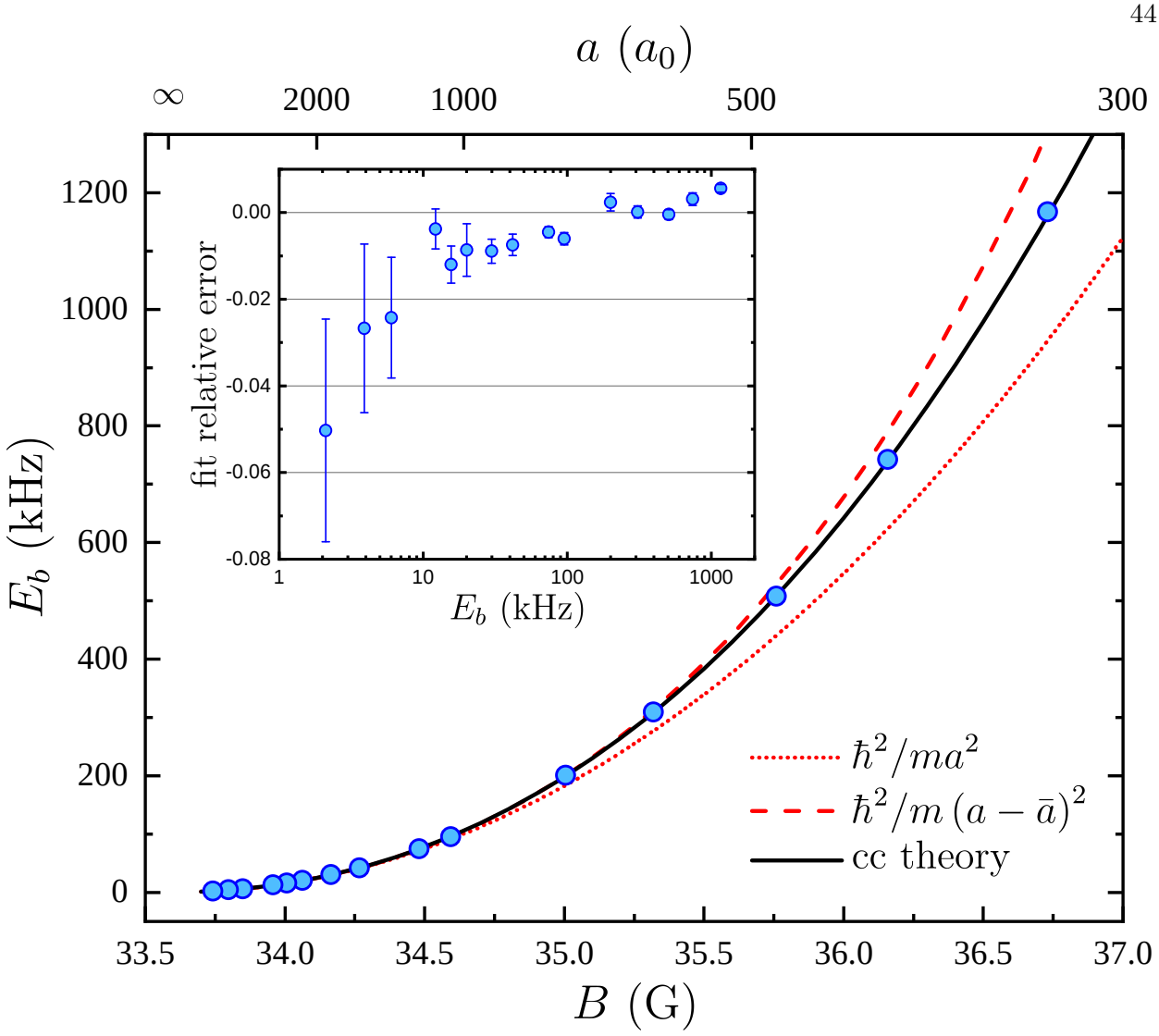

Figure 5.8a: The initial fit of our binding energy data to a coupled-channel (cc) theory model, without accounting for the confinement shift. We require the cc model to describe E_b because universal expressions (dashed and dotted curves) are insufficient for our intermediate-strength resonance. Error bars on the data points are not resolvable on the scale of the figure. The inset shows our fractional residuals, which express the difference between our experimental points and the fitting curve. Note the systematically negative fit residuals for our smallest E_b data. This error is accounted for by the confinement shift (see Figure 5.8b).

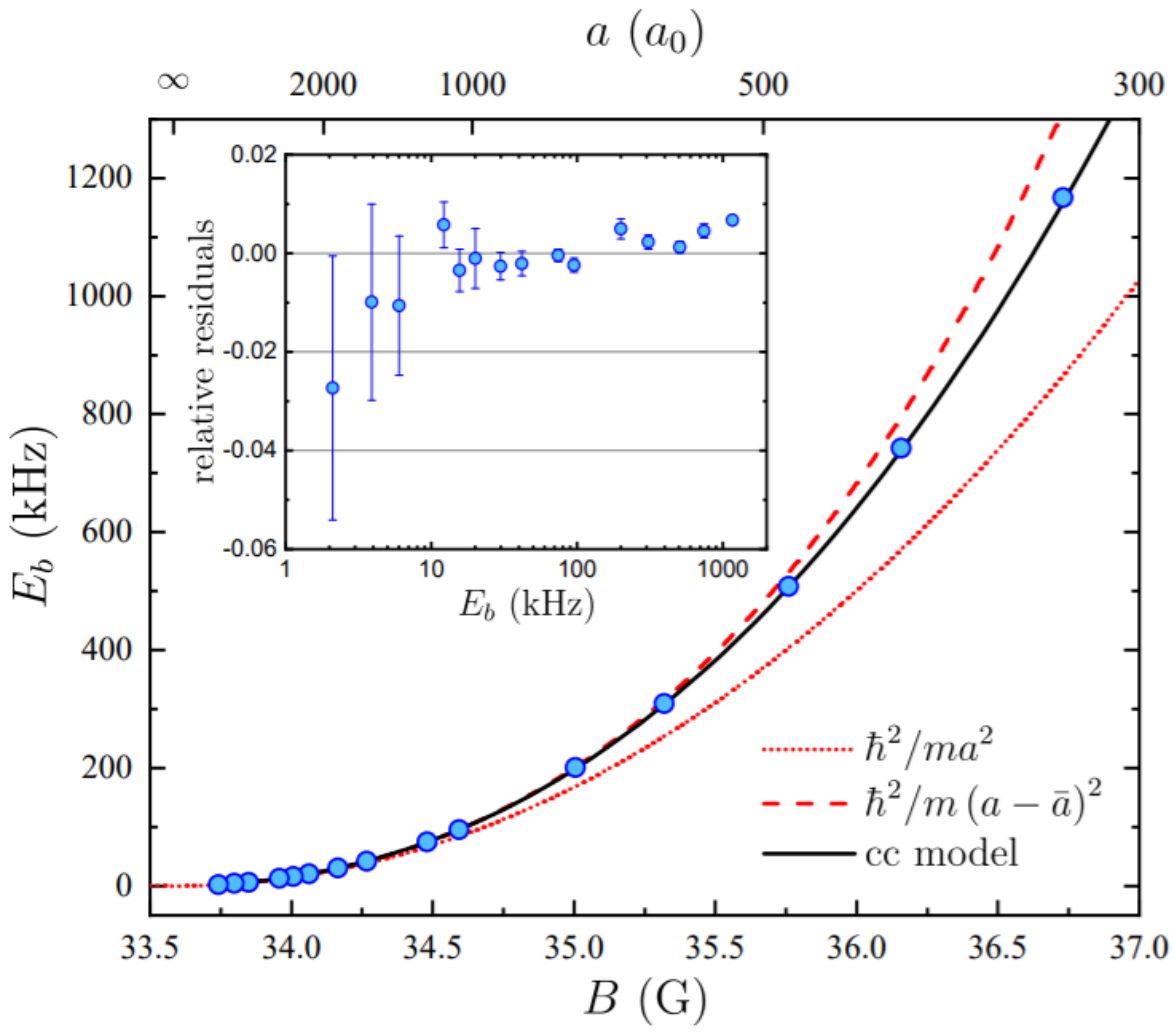

Figure 5.8b: The final fit of our binding energy data to a coupled-channel (cc) theory model, where we have accounted for the confinement shift. We require the cc model to describe E_b because universal expressions (dashed and dotted curves) are insufficient for our intermediate-strength resonance. Error bars on the data points are not resolvable on the scale of the figure. The inset shows our final fractional residuals, which express the difference between our experimental points and the fitting curve. Note how the fit residuals for our smallest E_b data here show much more agreement with zero residual than in Figure 5.8a. This demonstrates the importance of accounting for the confinement shift to our data.

Chapter 6

Conclusion and Future Directions

In this thesis, I have combined an introduction to the theory of two-particle scattering physics and Feshbach resonances with an experimental description of how ultracold gases (and specifically Feshbach molecules) are produced and measured, and described the particular work that I did in accounting for the confinement shifts on our measured binding energies of ^{39}K Feshbach molecules. The work presented in this thesis was a small part of our broader effort towards precision measurements of few-body physics in an interacting quantum gas. Over my time as a part of the lab, we went from struggling to reach degeneracy with ^{39}K to forming a solid foundation in two-and three-body measurements that will continue to develop and expand for years to come.

There are still many open questions left to explore in the realm of few-body and universal physics with ultracold Bose gases. In particular, this thesis focused only on our work characterizing the two-body physics that arises from Feshbach resonances, but there is a rich spectrum of three-body and four-body physics tied to Feshbach resonances which has yet to be fully and precisely characterized. Common problems with previous work in this area include failing to account for systematic effects such as finite temperature effects, incorrect density calibrations, and so on. Just as we have accounted for the confinement shift in this work, our lab aims to account for these systematic effects to obtain precision data that can serve as a benchmark for comparisons with theories. Such careful measurements are vital towards the goal of building a"ground up" understanding of quantum many-body physics through precise characterizations of quantum few-body physics.

Bibliography

[1] MA Baranov, Klaus Osterloh, and M Lewenstein. Fractional quantum hall states in ultracold rapidly rotating dipolar fermi gases. Physical review letters, 94(7):070404, 2005.

[2] Hans Bethe and Rudolf Peierls. Quantum theory of the diplon. Proceedings of the Royal Society of London. Series A-Mathematical and Physical Sciences, 148(863):146–156, 1935.

[3] Immanuel Bloch. Quantum coherence and entanglement with ultracold atoms in optical lattices. Nature, 453(7198):1016, 2008.

[4] Eric Braaten and H-W Hammer. Universality in few-body systems with large scattering length. Physics Reports, 428(5-6):259–390, 2006.

[5] Thomas Busch, Berthold-Georg Englert, Kazimierz Rzażewski, and Martin Wilkens. Two cold atoms in a harmonic trap. Foundations of Physics, 28(4):549–559, 1998.

[6] Roman Chapurin. Precise Measurements of Few-Body Physics in Ultracold 39k Bose Gas. PhD thesis, University of Colorado Boulder, 2019. Physics Graduate Theses & Dissertations. 289. https://scholar.colorado.edu/phys_gradetds/289.

[7] Roman Chapurin, Xin Xie, Michael J Van de Graaff, Jared S Popowski, Jose P D'Incao, Paul S Julienne, Jun Ye, and Eric A Cornell. A precision test of the limits to universality in few-body physics. arXiv preprint arXiv:1907.00729, 2019.

[8] Cheng Chin, Rudolf Grimm, Paul Julienne, and Eite Tiesinga. Feshbach resonances in ultracold gases. Reviews of Modern Physics, 82(2):1225, 2010.

[9] Cheng Chin and Paul S Julienne. Radio-frequency transitions on weakly bound ultracold molecules. Physical Review A, 71(1):012713, 2005.

[10] Jean Dalibard, Fabrice Gerbier, Gediminas Juzeliūnas, and Patrik Öhberg. Colloquium: Artificial gauge potentials for neutral atoms. Reviews of Modern Physics, 83(4):1523, 2011.

[11] Chiara d'Errico, Matteo Zaccanti, Marco Fattori, Giacomo Roati, Massimo Inguscio, Giovanni Modugno, and Andrea Simoni. Feshbach resonances in ultracold 39k. New Journal of Physics, 9(7):223, 2007.

[12] Richard J Fletcher, Raphael Lopes, Jay Man, Nir Navon, Robert P Smith, Martin W Zwierlein, and Zoran Hadzibabic. Two-and three-body contacts in the unitary bose gas. Science, 355(6323):377–380, 2017.

[13] Christopher J Foot et al. Atomic physics, volume 7. Oxford University Press, 2005.

[14] Jens Herbig, Tobias Kraemer, Michael Mark, Tino Weber, Cheng Chin, Hanns-Christoph Nägerl, and Rudolf Grimm. Preparation of a pure molecular quantum gas. Science, 301(5639):1510–1513, 2003.

[15] Eleanor Hodby, Sarah T Thompson, CA Regal, M Greiner, Andrew C Wilson, Deborah S Jin, Eric A Cornell, and Carl E Wieman. Production efficiency of ultracold feshbach molecules in bosonic and fermionic systems. Physical review letters, 94(12):120402, 2005.

[16] Kerson Huang and Chen Ning Yang. Quantum-mechanical many-body problem with hard-sphere interaction. Physical review, 105(3):767, 1957.

[17] Zbigniew Idziaszek and Tommaso Calarco. Analytical solutions for the dynamics of two trapped interacting ultracold atoms. Physical Review A, 74(2):022712, 2006.

[18] Maciej Lewenstein, Anna Sanpera, Veronica Ahufinger, Bogdan Damski, Aditi Sen, and Ujjwal Sen. Ultracold atomic gases in optical lattices: mimicking condensed matter physics and beyond. Advances in Physics, 56(2):243–379, 2007.

[19] Harold J Metcalf and Peter Van der Straten. Laser cooling and trapping of neutral atoms. The Optics Encyclopedia: Basic Foundations and Practical Applications, 2007.

[20] AJ Moerdijk, BJ Verhaar, and A Axelsson. Resonances in ultracold collisions of li 6, li 7, and na 23. Physical Review A, 51(6):4852, 1995.

[21] Torma Paivi and Sengstock Klaus. Quantum Gas Experiments: Exploring Many-Body States, volume 3. World Scientific, 2014.

[22] Christopher J Pethick and Henrik Smith. Bose–Einstein condensation in dilute gases. Cambridge university press, 2008.

[23] Cindy A Regal, Christopher Ticknor, John L Bohn, and Deborah S Jin. Creation of ultracold molecules from a fermi gas of atoms. Nature, 424(6944):47, 2003.

[24] Benno S Rem. The Road to the Unitary Bose Gas. PhD thesis, École Normale Supérieure de Paris - ENS Paris, 2013.

[25] Sanjukta Roy, Manuele Landini, Andreas Trenkwalder, Giulia Semeghini, Giacomo Spagnolli, Andrea Simoni, Marco Fattori, Massimo Inguscio, and Giovanni Modugno. Test of the universality of the three-body efimov parameter at narrow feshbach resonances. Physical review letters, 111(5):053202, 2013.

[26] JT Stewart, JP Gaebler, and DS Jin. Using photoemission spectroscopy to probe a strongly interacting fermi gas. Nature, 454(7205):744, 2008.

[27] Eddy Timmermans, Paolo Tommasini, Mahir Hussein, and Arthur Kerman. Feshbach resonances in atomic bose–einstein condensates. Physics Reports, 315(1-3):199–230, 1999.

[28] Boudewijn Verhaar, Kurt Gibble, and Steven Chu. Cold-collision properties derived from frequency shifts in a cesium fountain. Physical Review A, 48(5):R3429, 1993.

[29] Huang Wu and Christopher J Foot. Direct simulation of evaporative cooling. Journal of Physics B: Atomic, Molecular and Optical Physics, 29(8):L321, 1996.

[30] Gerhard Zürn, Thomas Lompe, Andre Niklas Wenz, Selim Jochim, PS Julienne, and JM Hutson. Precise characterization of li 6 feshbach resonances using trap-sideband-resolved rf spectroscopy of weakly bound molecules. Physical review letters, 110(13):135301, 2013.

Appendix A

Reproducing ^{6}Li Confinement Shift Values

Figure A.1 below is the original table of the measured ^{6}Li Feshbach molecule dissociation frequency and computed confinement shifts from the Supplemental Materials of reference [30]. Figure A.2 is a table of the confinement shift and final binding energy results from my MATLAB program, given the scattering length values from reference [30]. In particular, the final four columns of Figure A.2 demonstrate that my program is effective at calculating the confinement shifts and corrected binding energies to well within experimental error, and in fact within the systematic error for the confinement shifts quoted by [30], which is given in the second parenthesis in the second to last column of Figure A.1.

dissociation freq. $\delta\nu$ [kHz]	initial a a_{12} [10^3 bohr]	final a a_{13} [10^3 bohr]	initial cs shift $\nu_{\text{cs-i}}$ [kHz]	final cs shift $\nu_{\text{cs-f}}$ [kHz]	cs shift ν_{cs} [kHz]	binding energy/h ν_{E_b} [kHz]
2.156 (8)(16)	18.34	-3.54(1)	0.006	0.359(1)	0.353 (3)(1)	1.803 (8)(17) (25)
4.697 (33)(16)	11.80	-3.69(2)	0.002	0.358(1)	0.356 (3)(1)	4.341 (33)(17) (50)
14.513 (6)(16)	6.54	-4.10(3)	0.002	0.357(1)	0.356 (3)(1)	14.157 (7)(17) (24)
127.461 (13)(16)	2.20	-8.71(22)	0.000	0.346(1)	0.346 (3)(1)	127.115 (14)(17) (31)

Figure A.1: A table of the measured dissociation frequencies, computed confinement shifts, and final binding energies for ^{6}Li, taken from the Supplemental Materials of reference [30]. The difference of the final and initial confinement shifts determines the total confinement shift ν_{cs}. The binding energy E_b is calculated from the difference between the measured dissociation frequency and the confinement shift. The second parenthesis in the second to last column gives the systematic error of the confinement shift of the final state, and the final parenthesis in the final column gives the total experimental error (sum of the statistical and systematic error).

dissociation freq. kHz	initial a (from paper 10^3 bohr	final a (from paper) 10^3 bohr	initial cs shift (from paper) kHz	my calculated initial cs shift kHz	final cs shift (from paper) kHz
2.156	18.34	-3.54	0.006	0.00518	0.359
4.697	11.8	-3.69	0.002	0.00188	0.358
14.513	6.54	-4.1	0.002	2.32054E-4	0.357
127.461	2.2	-8.71	0	-4.18411E-4	0.346

my calculated final cs shift kHz	total cs shift (from paper) kHz	my calculated total cs shi kHz	binding energy/h (from paper) kHz	my calculated binding energy/h kHz
		Col(F)-Col(D)	Col(A)-Col(H)	Col(A)-Col(I)
0.35901	0.353	0.35383	1.803	1.80217
0.35866	0.356	0.35678	4.341	4.34022
0.35768	0.356	0.35745	14.157	14.15555
0.34622	0.346	0.34663	127.115	127.11437

Figure A.2: A table of the reproduced confinement shifts and final binding energies for ^{6}Li from my MATLAB program. All columns marked (from paper) are the original values from reference [30] (reproduced in Figure A.1 above), and are included for reference with my reproduced values. The only inputs to my program were the scattering length values from [30] at which we wanted to compute the confinement shift.

Appendix B

MATLAB Program for Determining the Confinement Shift

For convenience, I have attached below the MATLAB program that I wrote to determine the confinement shift to the binding energies of our ^{39}K Feshbach Molecules.

```
%% Program for determining the confinement shift for a given scattering length
% Jared Popowski

% To convert to a different atomic species/experimental setup, change the following
% in Parameter Setup as necessary:
% 1. eta (aspect ratio of the trap)
% 2. axialfreq (trap frequency in the axial direction)
% 3. zeropoint (zero point energy of the trap, h(f1+f2+f3)/2, where fi =
% frequency in ith direction)
% 4. m (mass of the atomic species)
%% INPUT SCATTERING LENGTH HERE (IN UNITS OF THE BOHR RADIUS)
bohrradius = 5.2917721067*10^-11;

testscatter = (-30*10^3)*bohrradius;

%% Parameter Setup
format long
eta = 28.64/117.3; %our experimental aspect ratio: 28.64/117.3, errors 0.66, 1.0.↙
"Best" values for 28.899/116.6
h = 6.6260755*10^-34; %Planck's constant
hbar = h/(2*pi);
axialfreq = 117.3;
energyunits = h*axialfreq;
zeropoint = h*0.5*(117.3+28.64+28.64);
dimensionlesszeropoint = zeropoint/energyunits;
AMU = 1.6605402*10^(-27);
m =  38.963707*AMU; % mass of 39K
lengthunits = sqrt(hbar/(2*pi*(m/2)*axialfreq));
Estart = -20;
Eend = 0.6; % This cannot exceed the value of dimensionlesszeropoint=0.7442!
Erange = Eend-Estart;
dE = 0.1;
numEpoints = 10000;
E = linspace(Estart,Eend,numEpoints+1); %To explore positive scattering lengths, make↙
Estart very small in magnitude
Epsilon = E-dimensionlesszeropoint;

%% Computes F(-Epsilon/2) and then the plotted scattering lengths according to eq. (22)↙
in Idziaszek PRA 2006.
% Also computes the free space energies according to eq. (2) in C. Chin's
% Feshbach resonance review paper.

seriesF = zeros(numEpoints+1,1);
fun = @(t,c) ((eta.*exp(-c.*t)./(sqrt(1-exp(-t)).*(1-exp(-eta.*t))))-1./(t.^(3/2)));
for x = 1:(numEpoints+1)
    seriesF(x,1) = integral(@(t)fun(t,-Epsilon(1,x)/2),0,Inf,'RelTol',1e-4,'AbsTol',1e-↙
11);
end
```

```
minusinversescatterlength = (1/sqrt(pi))*seriesF;
dimensionlessscatterlength = -1./(minusinversescatterlength);
scatterlength = dimensionlessscatterlength*lengthunits;


freespaceE = zeros(numEpoints+1,1);
for y = 1:(numEpoints+1)
    if scatterlength(y,1) < 0
        freespaceE(y,1) = 0;
    else
    freespaceE(y,1) = -(hbar^2)/(2*(m/2)*(scatterlength(y,1))^2);
    freespaceE(y,1) = freespaceE(y,1)/energyunits;
    end
end

%% Plots both the confined and free space energies of the universal bound states
plotvalues = horzcat(minusinversescatterlength,E.',freespaceE,E.'-freespaceE); %column↙
1 = -1/a, column 2 = confined E values, column 3 = free space E values, column 4 =↙
difference between energies

plot(plotvalues(:,1),plotvalues(:,2),'Color','b')%confined E values
title('K-39 Universal Bound State Energies')
xlabel('-1/a (units of 1/oscillator length)')
ylabel('E (units of hbar*omega_z)')
hold on
plot(plotvalues(:,1),plotvalues(:,3),'Color','r')%free space E values
legend('Confined','Free Space')


figure;
plot(plotvalues(:,1),plotvalues(:,4))
title('Difference Between Confined and Free Space Bound State Energies')
xlabel('-1/a [1/oscillator length]')
ylabel('E [hbar*omega_z]')


%% Calculate the Confinement Shift for the Given Scattering Length - Linear↙
Interpolation
dimensionlesstestscatter = testscatter/lengthunits;
minusinversetestscatter = -1/dimensionlesstestscatter;

[c index] = min(abs(plotvalues(:,1)-minusinversetestscatter));

if plotvalues(index,1)-minusinversetestscatter > 0.1 || plotvalues(index,1)-↙
minusinversetestscatter < -0.1
    disp('ERROR: Chosen scattering length outside of given energy bounds. Increase the↙
energy bounds in the program (Estart,Eend, and/or numEpoints) to include the scattering↙
length.')
else
%Linear interpolation between nearest scattering lengths to obtain energy.
```

```
%This looks complicated, but I explain how it works below.
%What follows assumes that the test
%scattering length has a corresponding energy that falls within the set
%energy range:
% 1. The program finds the index the nearest scattering length to the test
% scattering.
% 2. If the free space bound state energy is 0 at this scattering length,
% linearly interpolate between the closest confined energy points to the test↙
scattering
% length to get the "actual" confined energy at this scattering length. Compute the
% difference between the confined and free space bound state energies to find the↙
energy gap,
% and thus the confinement shift frequency.
% 3. If the free space bound state energy is not zero at this scattering
% length, linearly interpolate between the closest confined AND FREE SPACE
% energy points to find the "actual" confined and free space energies at
% this scattering length. As before, compute the difference between the
% confined and free space energies to find the energy gap and hence the
% confinement shift frequency.
    if plotvalues(index,3) ~= 0
        if plotvalues(index,1) > minusinversetestscatter
        confinedslope = (plotvalues(index,2)-plotvalues(index-1,2))/(plotvalues(index,↙
1)-plotvalues(index-1,1));
        confinedinterpolatedenergy = plotvalues(index-1,2)+confinedslope*↙
(minusinversetestscatter-plotvalues(index-1,1));
        freespaceslope = (plotvalues(index,3)-plotvalues(index-1,3))/(plotvalues(index,↙
1)-plotvalues(index-1,1));
        freespaceinterpolatedenergy = plotvalues(index-1,3)+freespaceslope*↙
(minusinversetestscatter-plotvalues(index-1,1));
        energydifference = confinedinterpolatedenergy-freespaceinterpolatedenergy;
        confinementshift = (energydifference*energyunits)/(h*1000) %Prints out the↙
confinement shift for the given point, in kHz
        disp('Confinement shift measured in kHz.')
        else
        confinedslope = (plotvalues(index+1,2)-plotvalues(index,2))/(plotvalues↙
(index+1,1)-plotvalues(index,1));
        confinedinterpolatedenergy = plotvalues(index,2)+confinedslope*↙
(minusinversetestscatter-plotvalues(index,1));
        freespaceslope = (plotvalues(index+1,3)-plotvalues(index,3))/(plotvalues↙
(index+1,1)-plotvalues(index,1));
        freespaceinterpolatedenergy = plotvalues(index,3)+freespaceslope*↙
(minusinversetestscatter-plotvalues(index,1));
        energydifference = confinedinterpolatedenergy-freespaceinterpolatedenergy;
        confinementshift = (energydifference*energyunits)/(h*1000) %Prints out the↙
confinement shift for the given point, in kHz
        disp('Confinement shift measured in kHz.')
        end
    else
        if plotvalues(index,1) > minusinversetestscatter
        slope = (plotvalues(index,2)-plotvalues(index-1,2))/(plotvalues(index,1)-↙
```

```
plotvalues(index-1,1));
        interpolatedenergy = plotvalues(index-1,2)+slope*(minusinversetestscatter-↙
plotvalues(index-1,1));
        energydifference = interpolatedenergy-plotvalues(index,3);
        confinementshift = (energydifference*energyunits)/(h*1000) %Prints out the↙
confinement shift for the given point, in kHz
        disp('Confinement shift measured in kHz.')
        else
        slope = (plotvalues(index+1,2)-plotvalues(index,2))/(plotvalues(index+1,1)-↙
plotvalues(index,1));
        interpolatedenergy = plotvalues(index,2)+slope*(minusinversetestscatter-↙
plotvalues(index,1));
        energydifference = interpolatedenergy-plotvalues(index,3);
        confinementshift = (energydifference*energyunits)/(h*1000) %Prints out the↙
confinement shift for the given point, in kHz
        disp('Confinement shift measured in kHz.')
        end
    end
end
```